New composite bio- and isotope stratigraphies spanning the Middle Eocene Climatic Optimum at tropical ODP Site 865 in the Pacific Ocean

Kirsty M Edgar[a,b], Steven M Bohaty[c], Helen K. Coxall[d], Paul Bown[e], Sietske J. Batenburg[f], Caroline H. Lear[a] and Paul N. Pearson[a]

[a]School of Earth and Ocean Sciences, Cardiff University, Cardiff, CF10 3AT, UK
[b]School of Geography, Earth and Environmental Sciences, University of Birmingham, B15 2TT, UK
[c]Ocean and Earth Science, National Oceanography Centre Southampton, University of Southampton, SO14 3ZH, UK
[d]Department of Geological Sciences, Stockholm University, SE-106 91, Stockholm Sweden
[e]Department of Earth Sciences, University College London, London, WC1E 6BT, UK
[f]University of Rennes, CNRS, Géosciences Rennes, UMR 6118, 35000 Rennes, France

Corresponding author

Kirsty M Edgar - E: k.m.edgar@bham.ac.uk. T: +44 (0) 121 414 6163. School of Geography, Earth and Environmental Sciences, Aston Webb Block A, University of Birmingham, Edgbaston, B15 2TT, UK

Abstract

The Middle Eocene Climatic Optimum (MECO) at ca. 40 Ma is one of the largest of the transient Eocene global warming events. However, it is relatively poorly known from tropical settings as few sites span the entirety of the MECO event and/or host calcareous microfossils, which are the dominant proxy carrier. Ocean Drilling Program (ODP)

Pacific Ocean Site 865 in the low-latitude North Pacific (Allison Guyot) has the potential to provide a useful tropical MECO reference but detailed stratigraphic and chronological constraints needed to evaluate its completeness were previously lacking. We have addressed this deficit by generating new high-resolution biostratigraphic, stable isotope and X-ray fluorescence (XRF) records spanning the MECO interval (~38.0–43.0 Ma) in two holes drilled at Site 865. XRF records of Sr/Ca, Ba/Sr and Fe allow correlation between holes and reveal pronounced rhythmicity, enabling us to develop the first composite section for Holes 865B and 865C and a preliminary cyclostratigraphy for the MECO. Using this new framework, the sedimentary record is interpreted to be continuous across the event, as identified by a pronounced transient $\delta^{18}O$ shift of ~0.8‰. Calcareous microfossil biostratigraphic events from widely used zonation schemes are recognized, with generally good agreement between the two holes, highlighting the robustness of the new composite section and allowing us to identify planktic foraminiferal Zones E10-E15 and calcareous nannofossil Zones NP15–18. However, discrepancies in the relative position and ordering of several primary and secondary bioevents with respect to published schemes are noted. Specifically, the stratigraphic highest occurrences of planktic foraminifera *Acarinina bullbrooki, Guembelitrioides nuttalli*, and *Morozovella aragonensis,* and calcareous nannofossils *Chiasmolithus solitus* and *Sphenolithus furcatolithoides* and the lowest occurrence of *Cribrocentrum reticulatum,* all appear higher in the section than would be predicted relative to other bioevents. We also note conspicuous reworking of older microfossils (from planktic foraminiferal Zones E5-E9 and E13) into younger sediments (planktic foraminiferal Zones E14-15) within our study interval consistent with reworking in the topmost ~30 m of the site. Regardless of reworking, the high-quality, XRF records enable decimeter scale correlation between holes and highlight the potential of Site 865 for constraining tropical environmental and biotic changes, not just across the MECO but also throughout the Paleocene and early-middle Eocene.

Keywords

MECO, planktic foraminifera, biostratigraphy, XRF, benthic isotope stratigraphy

Introduction

The transition from peak Eocene 'greenhouse' conditions at ~50–52 Ma to the onset of the icehouse at ~34 Ma is punctuated by a number of transient climate events (e.g., Bohaty et al., 2009; Edgar et al., 2007; Sexton et al., 2011; Zachos et al., 2008). The most pronounced of these is the MECO event at ~40 Ma that represents a temporary reversal in the long-term Eocene global cooling trend (Bohaty and Zachos, 2003; Bohaty et al., 2009). The MECO event is characterized by ocean warming of ~3–6°C (Bijl et al., 2010; Bohaty et al., 2009; Boscolo Galazzo et al., 2014; Edgar et al., 2010), ocean acidification evidenced by >1 km shoaling of the Pacific calcite compensation depth (CCD), and shifts in the global carbon cycle (Bohaty et al., 2009; Pälike et al., 2012). Biotic responses vary across the event, impacting floral and faunal composition, body size, and ecology in the deep and surface ocean globally (e.g., Arreguín-Rodríguez et al., 2016a; Boscolo Galazzo et al., 2015; Cramwinckel et al., 2019; Edgar et al., 2013; Luciani et al., 2010; Möbius et al., 2015; Witkowski et al., 2014).

The MECO is well known from mid- and high-latitude sites (e.g., ODP Sites 689, 690, 702, 748, 738, 1051, 1172 and 1263 and the Alano, Contessa Highway and Monte Cagnero sections in Italy), many of which also are characterized by good stratigraphic age control, comprehensive isotope stratigraphies and carbonate rich sediments yielding microfossil useful for proxy reconstructions (Bijl et al., 2010; Bohaty and Zachos, 2003; Bohaty et al., 2009; Boscolo Galazzo et al., 2014; Edgar et al., 2010; Jovane et al., 2007; Rivero-Cuesta et al., 2019; Savian et al., 2013; Spofforth et al., 2010). However, we currently lack a low-latitude site that unambiguously spans the pre-MECO, MECO and post-MECO intervals and has continuous carbonate sedimentation uninterrupted by CCD or lysocline shoaling, thus hindering our understanding of environmental and biotic responses in the tropics.

Of the sites that do exist, ODP Site 1260 in the equatorial Atlantic has a high-resolution stable isotope stratigraphy that has been placed onto an orbitally tuned age model providing unprecedented age control (Edgar et al., 2010; Westerhold and Röhl, 2013). However, interpretation of the MECO at this site is complicated by the lack of a clear return to higher $\delta^{18}O$ values following the event and a hiatus which truncates the upper portion of the record (Edgar et al., 2010; Shipboard Scientific Party, 2004). IODP Site U1333 in the equatorial Pacific Ocean also has good age control with both a comprehensive magnetic stratigraphy and an orbitally tuned age model across the whole of the MECO interval (Expedition 320/321 Scientists, 2009; Westerhold et al., 2014), but its relatively deep paleo-water depth (~3.5 km), coupled with a relatively shallow Pacific CCD in the middle Eocene, resulted in little or no carbonate preservation across the peak of the event, preventing detection of its true magnitude (Expedition 320/321 Scientists, 2009; Pälike et al., 2012; Westerhold et al., 2014). Furthermore, no planktic foraminifera are present across the entire MECO interval at Site U1333 to constrain surface-water conditions. Similarly, at shallower ODP Site 1209 (~2 km paleo-water depth) in the subtropical North Pacific Ocean (Dutton et al., 2005) the interval containing the MECO has poor carbonate microfossil preservation, very low sedimentation rates and thus, poor age control (Dawber and Tripati, 2011; Shipboard Scientific Party, 2002).

Equatorial Pacific ODP Site 865 is an older site that has been rather neglected in Eocene paleoceanographic studies. Drilled on Allison Guyot in 1992 on ODP Leg 143, the recovered cores sample the pelagic sediment drape (~200 m thick at the centre, ~140 m at Site 865 which was drilled off-centre) that accumulated during much of the Paleogene and early Neogene. Existing studies reveal the sediments to comprise a succession of Paleocene to Miocene foraminiferal-nannofossil ooze and foraminiferal sands (Shipboard Scientific Party, 1993a). The relatively shallow paleo-water depths (<2 km) on the guyot top maximizes the preservation potential of carbonate microfossils, thus avoiding problems of CCD and lysocline shoaling encountered elsewhere at deeper sites (e.g., IODP Site U1333). Several Paleogene-focused studies have highlighted the potential of this site for paleoceanographic and evolutionary studies (Arreguín-Rodríguez et al., 2016b; Bralower et al., 1995; Coxall et al., 2000; Edgar et al., 2015; Norris and Nishi, 2001; Pearson and Ezard, 2014; Pearson and Palmer, 2000; Tripati et al., 2003), but most of the high-temporal resolution work has focused on the Paleocene-Eocene Thermal Maximum (PETM) (Kelly et al., 1996; Kozdon et al., 2011; Kozdon et al., 2013; Tripati and Elderfield, 2004) since ODP Site 865 is one of the few open ocean sites with carbonate present throughout the event.

Middle Eocene sediments at Site 865 have not received much attention for paleoceanographic studies, in large part because of: (1) poor quality of shipboard physical property records preventing the development of a composite section necessary to develop continuous stratigraphic sections, (2) the lack of magnetic reversal or cyclostratigraphy for age control, and (3) evidence for reworking of calcareous microfossils, e.g., across the PETM onset and in the upper portions of the sediment column (Bralower and Mutterlose, 1995; Kelly et al., 1998; Shipboard Scientific Party, 1993a). Reworking and winnowing of sediment is an acknowledged problem of guyot-top sites where ocean currents can be locally intensified by the topography (Pearson, 1995). However, evolutionary work, has demonstrated that the calcareous microfossils, are diverse and abundant, albeit recrystallized (Edgar et al., 2015; Pearson et al., 2001; Sexton et al., 2006) providing an apparently complete sequence of tropical Paleogene biomarkers and their lineage evolution (Coxall et al., 2000; Norris and Nishi, 2001; Pearson and Ezard, 2014). Importantly, existing biostratigraphic assessments for Holes 865B and 865C identify planktonic foraminiferal Zone E12, defined by the total range of *Orbulinoides beckmanni* and spanning the MECO interval, and calcareous nannofossil Zone CN15/NP16, although there are large (~1 m) recovery gaps between cores (Bralower and Mutterlose, 1995; Shipboard Scientific Party, 1993a). Core photos indicate the presence of carbonate-rich sediments throughout the entire interval of interest (i.e., there is no evidence of a clay horizon) providing a promising target for geochemical and plankton assemblage work worth further investment (Edgar et al., 2015; Pearson and Palmer, 2000; Shipboard Scientific Party, 1993a).

Here we take the first step towards developing the ODP Site 865 MECO sequence as a palaeoceanographic reference by adding new data sets that allow development of a refined and detailed chronostratigraphy for the site. This involves high-resolution X-ray fluorescence (XRF) core scanning, benthic foraminiferal stable isotope ($\delta^{13}C$ and $\delta^{18}O$), and planktic foraminiferal and calcareous nannofossil biostratigraphic data across the MECO interval at the site. These data are combined with published calcareous nannofossil datums (Bralower and Mutterlose, 1995) to: [1] generate the first composite sedimentary section across the middle Eocene interval of Site 865, [2] identify and constrain the isotopic character of the MECO in the Pacific Ocean, and [3] determine the position of key biostratigraphic datums relative to the MECO event.

2. Materials and Methods

2.1 Regional Setting

ODP Site 865 was recovered during ODP Leg 143 and is located on Allison Guyot in the western North Pacific Ocean at 18° 26.410'N, 179° 33.339'W and a modern water depth of 1516 m (Shipboard Scientific Party (1993a); Fig. 1). This guyot is just one of a number of similar flat topped volcanic seamounts in the region formed during the Cretaceous (e.g., Resolution and Wodejebato Guyots), rising up several km from the surrounding abyssal (>4 km) seafloor (Matthews et al., 1974; Shipboard Scientific Party, 1993b). Three holes were drilled at Site 865 (A–C) with middle Eocene sediments only recovered in Holes B and C, which were cored to try and create a continuous record of this interval. The middle Eocene sequence at Site 865 is positioned at shallow burial depths (<100 m) with no significant Quaternary cover. The foraminiferal nannofossil ooze and foraminiferal sands are reconstructed to have been deposited at ~1300–1500 m paleo-water depth based on benthic foraminiferal assemblages (Shipboard Scientific Party, 1993a) in a fully pelagic ocean gyre setting characterized by year round thermal stratification (Pearson et al., 2001).

2.2 X-Ray Fluorescence (XRF) Scanning

XRF data are routinely employed for stratigraphic correlation and the construction of high-resolution composite depth scales because of their higher signal-to-noise ratio and more consistent hole-to-hole character than shipboard physical property measurements (Röhl and Abrams, 2000). Prior to XRF analysis, the top ~0.5 cm of the split section surface of the archive halves was scraped off with a glass slide. This revealed bioturbation structures, indicating that this interval did not have significant coring disturbance (as might be expected from the foraminifera-ooze lithologies and the massive appearance of the unprepared cores). Using an Avaatech XRF scanner with a Canberra X-PIPS SDD, Model SXD-150-500 X-ray detector, a suite of element (including Fe, Ca, Sr, and Ba) intensity data were collected every 2 cm down-core with a constant spot size (cross core slot = 12 mm, down-core slit = 10 mm) using a 6 or 10 second count time at 30 and 50 kV, respectively, on the split surface of the archive half of each section using the TAMU ODASES XRF scanner at the International Ocean Discovery Program (IODP) Gulf Coast Core Repository. We measured the elemental composition of sediments that encompassed planktic foraminiferal Zone E12 from ODP Cores 865B-4H and 5H (27.52–44.58 mbsf) and Sections 865C-4H-1 to 6H-2 (22.34–42.80 mbsf) in order to capture overlapping sections and construct a composite splice. All XRF elemental data are reported in Supplementary Table 1.

2.3 Cyclostratigraphy

To investigate if orbital forcing drove patterns in the elemental data records, the Fe intensity data and the natural logarithm of Sr/Ca, ln(Sr/Ca), as measured at 30 kV, was subjected to time series analyses. The Fe intensity data were selected to allow comparison with published datasets (Westerhold and Röhl, 2013), and the ln(Sr/Ca) record for its low signal to noise ratio (see Section 3.1). Records were evenly sampled and periodicities larger than 7 m were removed in the program *AnalySeries* (Paillard et al., 1996). Spectral analyses were performed with *Redfit 3.8* (Schulz and Mudelsee, 2002) using a Welch window. The behavior of periodicities over the length of the dataset was investigated by evolutive harmonic analysis with the astrochron package in R (Meyers, 2014), using a window length of 5.5 m for ln(Sr/Ca) and 6 m for Fe intensity. The Fe record displays a stronger imprint of short-term (<1 m) variability than the ln(Sr/Ca) record. To test whether the observed cycle hierarchy in the Fe record can be confidently linked to an orbital origin, the interval with most persistent periodicities as identified in the evolutive spectrum, between 32.5 and 44.5 amcd, was investigated with the average spectral misfit (ASM) method in *astrochron* (Meyers, 2014). Bandpass filters were applied to the datasets centered at periodicities of 1.9 m and 50 cm with broad bandwidths of 1/3 of the center frequency. The ln(Sr/Ca) record displays a stronger imprint of longer (>1 m) periodicities than the Fe record, with minima in the 1.9-m bandpass filter of ln(Sr/Ca) generally coinciding with maxima in the 1.9-m bandpass filter of Fe. High Fe intensities generally coincide with intervals of higher variability in the Fe record, which are likely controlled by a larger amplitude of variation in the orbital forcing parameters, during eccentricity maxima. In concordance with the approach of (Westerhold and Röhl, 2013), we consider eccentricity maxima to coincide with maxima in the Fe record, and therefore minima in the ln(Sr/Ca) record. A tentative orbital tuning was established by (i) anchoring the maximum in the 1.9-m bandpass filter of ln(Sr/Ca) to the 405 kyr eccentricity minimum at 40.5 Ma in the La2011 eccentricity solution (Laskar et al., 2011), and (ii) connecting consecutive maxima in the 1.9-m bandpass filter of ln(Sr/Ca) to 405 kyr eccentricity minima.

2.4 Planktic foraminiferal and calcareous nannofossil biostratigraphy

Biostratigraphic analysis was conducted on samples spanning the inferred MECO interval to identify both primary bioevents defining planktic foraminiferal zones and key secondary datums as defined by Berggren and Pearson (2005) and Wade et al. (2011). Biostratigraphic samples were taken between Sections 865B-4H-3 and -5H-2, (~30.60–39.98 meters below sea floor, mbsf) in Hole 865B and between Sections 865C-4H-1 and -6H-2 (~22.35–44.05 mbsf) in Hole 865C, initially at relatively low resolution but increasing to ~10–20 cm spacing close to key datums. The position of planktic foraminifer datums outside of the studied sample set were determined using shipboard biostratigraphic residues with one sample per core section (every ~1.5 m) and are as presented in Figure 1 of Pearson and Ezard (2014) from Coxall (*unpub.*). Taxonomy follows Pearson et al. (2006). We also present calcareous nannofossil datums determined by Bralower and Mutterlose (1995) and new nannofossil data based on analysis of an additional 20 samples from Sections 865B-4H-3 to -5H-1 and Sections 865C-4H-5 to -5H-5. We use Top (T) and Base (B) to describe the highest and lowest occurrences of taxa, and Top and Base common (Tc and Bc) for the highest and lowest common occurrences, respectively. Representative specimens of key biostratigraphically important taxa were selected for Scanning Electron Microscope

(SEM) analysis. Specimens were gold coated prior to analysis and SEM imaging was conducted on a Philips XL-30 Environmental SEM at the University of Birmingham.

2.5 Stable carbon and oxygen isotope measurements

Benthic foraminiferal stable isotope ($\delta^{13}C$ and $\delta^{18}O$) data were generated from the epifaunal taxon *Nuttallides truempyi* following the taxonomic concept of Holbourn et al. (2013). Foraminifers were picked from the 250–300 μm sieve size fraction and cleaned by ultrasonication to remove any loose fine material prior to stable isotope analysis. All stable isotope measurements were determined using a Thermo Scientific Delta V Advantage mass spectrometer coupled to a Gas Bench II in the School of Earth and Ocean Sciences at Cardiff University and are reported relative to the Vienna Pee Dee Belemnite (VPDB) standard. External analytical precision for $\delta^{13}C$ and $\delta^{18}O$ analyses is 0.06 and 0.07‰, respectively. No species-specific corrections are applied. Stable isotope data for Holes 865B and 865C are reported in Supplementary Tables 2 and 3, respectively.

3. Results

3.1. XRF data

Despite initial concerns about coring disturbance and the lack of clear signals in the shipboard physical property datasets (Shipboard Scientific Party, 1993a), pronounced cyclicity is evident in the high-resolution XRF records throughout the study interval aiding correlation between holes (Fig. 2; Supplementary Table 1). Sr/Ca and Ba/Ca data are the most useful parameters for correlation because of the higher signal-to-noise ratio compared to other elemental ratios, e.g., Fe/Sr. These datasets enabled the construction of an unambiguous composite depth scale spanning a ~25-m interval between ~22 and 47 mbsf for the first time at Site 865 (Tables 1 and 2). This is the first core splice (and thus, official meters composite depth (mcd) scale) available for any interval at Site 865. The biggest difference between the new mcd scale and the shipboard mbsf depth scale is that the core recovery gap between Cores 865C-4H and -5H has increased from ~1 to >3 m indicating that significant offsets must be applied. In order to maximize the sample material available for study, out-of-splice intervals were also correlated to the in-splice intervals through development of an 'adjusted' meters composite depth (amcd) scale (Tables 3 and 4; Fig. 2). This new amcd scale only applies to the intervals for which XRF are collected and thus, some of the bioevents reported in this study fall outside of this. This was achieved by aligning clearly identifiable common features in each hole, and defining mapping pairs (Tables 3 and 4) by stretching/squeezing of the out-of-splice core segments to match the in-splice intervals (Fig. 2). All interpretations below are considered relative to the final composite amcd scale. Note that it was not possible to align all features in the elemental records because of distortion (contraction and expansion) within each core. Also, since the intent of this work is to generate a composite section across the MECO interval, we do not focus here on the possible environmental implications of the XRF records.

3.2 Cyclostratigraphy

Spectral analysis of the ln(Sr/Ca) record by Redfit displays the most prominent periodicities at 1.9 m and 73 cm, and additional periodicities at 3.0 m, 2.4 m, 78 cm and 40 cm above the 95% confidence level, and at 60 cm above the 90% confidence level (Fig. 3). In the Fe record, periodicities above the 95% confidence level are detected at 6.3 m, 1.9–1.2 m and 63 cm (Fig. 3), with an additional periodicity of 49 cm above the 80% confidence level. Evolutive analyses track the behavior of the ~1.9 m and 40–78 cm periodicities over the length of the record, revealing reduced power at depths around 32.5 and 39.5 amcd. ASM analysis of the Fe intensity record from 32.5 to 44.5 m reveals a hierarchy of periodicities likely corresponding to an orbital imprint at a sedimentation rate of 0.46 cm/kyr (Supplementary Fig. 1). This is in close agreement with the average sedimentation rate obtained from tuning to the 405-kyr eccentricity cycle at 0.48 cm/kyr on average over the entire record. A sedimentation rate of 0.48 cm/kyr would translate the periodicity of 1.9 m, which is strongly present in the ln(Sr/Ca) record, to a duration of 406 kyr, which is close to the periodicity of long eccentricity at 405 kyr.

3.2 Planktic foraminiferal biostratigraphy

All of the samples analysed contain abundant recrystallised or 'frosty' planktic foraminifera (See Fig. 6 and Edgar et al. (2015) for images of wall cross sections). The assemblages are diverse and typical of tropical middle Eocene low latitude environments. The dominant genera are *Acarinina, Morozovelloides*, *Turborotalia, Globigerinatheka* and *Subbotina,* with minor but conspicuous contributions from *Hantkenina, Guembelitrioides, Globanomalina,* and *Pseudohastigerina*. Thus, the (sub)tropical planktic foraminifera zonation scheme of Berggren and Pearson (2005) can easily be applied at this site and, unusually, a complete sequence of Eocene biomarkers and biozones can be identified. From the pattern of evolutionary bioevents recognized we identify planktic foraminiferal Zones E10–E15 within the study interval (Table 5; Fig. 5). Images of planktic foraminiferal species of biostratigraphic significance are shown in Figure 4.

The planktic foraminiferal biostratigraphic data serve two purposes: (i) comparison of bioevents in Holes 865B and 865C to provide a check on XRF-based hole-to-hole correlations, and (ii) critical age control for this site. The relative sequence and depths of planktic foraminiferal datums in Holes 865B and 865C are in relatively good agreement with one another on the new amcd scale, indicating no major misalignments based on the XRF correlations. The top of *G. semiinvoluta,* defining the base of Zone E15, falls in samples outside of the new splice (Table 5), occurring at 20.35±0.10 mbsf in Hole 865B and at 21.57±0.79 mbsf in Hole 865C (and above 22.37 amcd). Small offsets between the two holes support the minimal composite depth offsets in the uppermost cores (<0.78 m; Tables 1, 2 and 5; Figure S2). Unfortunately reworking of older into younger material is evident in the topmost samples investigated here (<31 amcd; Fig. 3) specifically early middle Eocene material is reworked into middle and late Eocene sediments. The most noticeable example of this is in the overlapping occurrences of *Globigerinatheka semiinvoluta* with the large A*carinina (e.g., A. praetopilensis* and *A. mcgowrani)* and *Morozovelloides (M. crassatus* and *M. lehneri),* and even *Morozovella aragonenesis* (from Zones E5-9) in Sections 865C-4H-1 to -4H-4. Reworking is not immediately evident in the topmost samples of the high-resolution sample set from Hole 865B. Fortunately reworked specimens are relatively easy to discern as they typically have a distinctive brown/orange stain, may contain small flecks of pyrite and are more poorly preserved, e.g., fragmented. We find no obvious evidence of down-hole contamination.

The evident reworking has several consequences for the biostratigraphic zonation. First, the Top of *M. crassatus* used to define the base of Zone E14 was not confidently identified here because significant numbers of individuals are present in both Cores 865B-3H and 865C-3H. Thus, the base of *G. semiinvoluta,* which is calibrated to the same age as the Top of *M. crassatus* was used to approximate the base of Zone E14 instead (27.61±1.01 mbsf in Hole 865B and 26.34±0.07 amcd in Hole 865C). The slight difference between the two horizons may reflect its relative rarity of this taxon and difficulties distinguishing *G. semiinvoluta* from its immediate ancestor *G. mexicana* at the base of its range (Premoli Silva et al., 2006) or that Cores 865B-3H and 865C-3H fall outside of the new amcd scale. In contrast, the Top of *O. beckmanni* is an easily identifiable datum that defines the base of Zone E13 and is well constrained in Hole 865B (32.14±0.06 amcd). This datum, however, falls in the core gap between Cores 865C-4H and -5H (33.00±2.10 amcd), and hence there is a large depth uncertainty on this datum in Fig. 5. The Base of *O. beckmanni,* and thus Zone E12, can be more difficult to define because there is a continuous chronocline from its ancestor *G. euganea* and there is no simple taxonomic discrimination, especially as the holotype is a relatively un-extreme form (Edgar et al., 2010; Premoli Silva et al., 2006) but here we find highly developed spherical forms in the lowermost part of the species range at 40.89±0.07 amcd and 41.03±0.05 amcd in Holes 865B and 865C, respectively. The Top of *A. bullbrooki* occurs ~4 m above the first occurrence of *O. beckmanni* at both sites (36.30±0.06 in Hole 865B and 37.13±0.05 amcd in Hole 865C) with highly quadrate 'classic' *A. bullbrooki* forms (Berggren et al., 2006) present that are not obviously reworked. This provides a further informal correlative horizon and a check on the correlation between Holes 865B and 865C. Whilst not official biozone markers for this interval of the Eocene, the *Hantkenina* assemblage at this site is very well developed and these taxa may be useful accessory markers (Coxall and Pearson 2006). For instance, we note that *Hantkenina australis* appears in samples at ~43 amcd coincident with a pronounced isotopic excursion (Fig. 5, possible C19r event).

The lower portion of the study interval is assigned to Zones E10 and E11. The top of *Guembelitrioides nuttalli,* which defines the base of Zone E11, occurs at 46.62±0.1 amcd in Hole 865C but was not defined in Hole 865B (as it fell outside of the available sample set). Notably, a small number of individuals that share the morphology of *G. nuttalli* with the distinctive high spire, globular chambers and a pronounced rim (Olsson et al., 2006) but which lack supplementary apertures on the spiral side are present sporadically much higher in the site up to ~22 amcd (Fig. 4e-f). The extinction of the distinctive taxon *Morozovella aragonensis* defining the base of Zone E10 falls outside of the new splice at 48.01±0.76 and 47.99±3.94 mbsf in Holes 865B and 865C, respectively. In Hole 865C, this corresponds to the extinction occurring below 47.51 amcd. The base of the secondary marker species *G. index* occurs at 62.10±0.50 mbsf in Hole 865B, and the bases of *G. index* and *M. lehneri* occur at 56.96±0.56 mbsf in Hole 865C. These datums typically occur in Zone E10 but occur well below the Top of *M. aragonensis* here (Table 5).

3.3. Calcareous nannofossil biostratigraphy

Calcareous nannofossils at Site 865 are moderately well preserved, showing signs of etching and/or recrystallization but most specimens are identifiable to species level throughout. Biostratigraphically important calcareous nannofossil occurrences from Bralower and Mutterlose (1995) that fall within our study interval are collated here and where possible translated onto the new amcd scale (Table 6). Marker species in Holes 865B and 865C on the new amcd scale are in broad agreement with one another, i.e., datums in both holes overlap in depth space (Fig. 6). Datums that don't quite overlap in terms of depth space are: *N. fulgens*, *R. (D.) bisectus* (>10 μm), *C. solitus,* and *S. furcatolithoides*. This is likely a function of the relative rarity of these taxa within the cores making it difficult to discern the highest or lowest true occurrence and/or that they are frequently overgrown making identification difficult (Bralower and Mutterlose, 1995). However, it is clear from the datums that fall outside of the interval incorporated in the new amcd scale in one or both Holes 865B and 865C (e.g., Bases of *Chiasmolithus oamaruensis* and *Reticulofenestra umbilicus* and Top of *C. gigas and C. grandis*) that bioevents in Cores 865B-3H and 865C-3H occur at similar levels indicating limited offsets between Holes 865B and 865C. More significant offsets of up to 5 m are present between Holes 865B and 865C from Cores 865B-7H and 865C-7H downwards indicating that significant adjustments are needed to align the two holes (Table 6).

Consistent with Bralower and Mutterlose (1995), calcareous nannofossil Zones NP15–18 (Martini, 1971)can be clearly identified at Site 865 (Table 6). On the more recent 'CNE' zonation scheme (Agnini et al., 2014), the interval encompassing CNE Zones 12–17 is identified but zones CNE14–16 cannot be differentiated. This is because the 'CNE' primary marker species are either: very rare at this site (*Cribrocentrum erbae*); occur in the same narrow window at ~28.5 amcd (T *Sphenolithus obtusus* and Bc *Cribrocentrum reticulatum,* defining the bases of Zones CNE16 and 14, respectively; Fig. 6); or between ~28-32 amcd appear out of sequence, e.g., the Bc *C. reticulatum* is very shallow compared, as are the T *S. furcatolithoides* and T *C. solitus,* which also show the largest offsets between the two holes.

3.4 Benthic foraminiferal stable isotope results

Benthic foraminiferal stable isotope records in both holes show similar patterns of change and absolute stable isotope values throughout the record, and are well aligned on the new amcd scale (Fig. 3). Benthic foraminiferal $\delta^{18}O$ values vary between 0.3 and 1.2‰ with a minimum $\delta^{18}O$ values initially recorded at ~43 amcd coincident with an abrupt shift of 0.7‰ to more negative $\delta^{13}C$ values. $\delta^{18}O$ and $\delta^{13}C$ values subsequently increase and then plateau between 42–37 amcd. At ~36.5 amcd, a second transient negative $\delta^{13}C$ excursion of ~1‰ occurs, which is closely followed by a ~0.8‰ shift to lower $\delta^{18}O$ values at 35 amcd. $\delta^{13}C$ values increase through this same interval and reach maximum values at 34 amcd. $\delta^{18}O$ values then gradually increase and $\delta^{13}C$ gradually decrease towards the top of the section at 24 amcd.

4. Discussion

4.1 Reworking

Reworking of older foraminifera (from Zone P14 now E13/14) into younger material in Cores 865B-1H to -3H was reported during shipboard analysis (Shipboard Scientific Party, 1993a) coinciding with the occurrence of relatively 'soupy' sediments with a high water content, a downcore transition to more cohesive sediments coincided with reduced reworking. We demonstrate that reworking of planktic foraminifera extends deeper than this transition but lessens considerably with increasing depth and is not immediately evident below Sections 865B 4H-3 or 865C 4H-4 (Figs 3 and 4). Only discrete time intervals are obviously mixed into younger sediments, i.e., reworked material is sourced from sediments deposited during Zone E13 (as we find re-worked *Morozovelloides* and *Acarinina* but not *O. beckmanni* from Zone E12) along with much older sediments from Zones E6–9. Reworking is less evident within nannofossil assemblages, but rare occurrences of *C. gigas* and *N. fulgens* occur several meters above their highest consistent occurrences in Cores 865B-3H and -4H and 865C-3H and -4H. These occurrences are consistent with remobilization of similar aged sediments and deposition within the same interval (Bralower and Mutterlose, 1995). Down-hole contamination was not obvious within planktic foraminifera assemblages but was problematic within calcareous nannofossil samples and was attributed to contamination from the saw used to split the cores and the high water content of the cores (Bralower and Mutterlose, 1995).

Reworking is very common in the pelagic cap sequences atop guyots drilled during ODP Legs 143 and 144 in the equatorial Pacific, with the most intense reworking reported in the lowermost ~40 m of pelagic sediments deposited above the drowned carbonate platforms related to changes in local hydrography (Pearson, 1995; Premoli Silva et al., 1993). Less intense reworking is also observed at higher (i.e., younger) levels in pelagic cap sequences and is more limited to discrete horizons and time intervals (Pearson, 1995; Watkins et al., 1995). Reworked material is likely sourced from the edges of the guyot top and transported towards the centre by intensification of bottom-water currents deflected up over the guyot as well as other localized hydrographic features common to these settings, ultimately helping to generate the characteristic low dome-shaped sediment stack found on many Pacific guyots (Genin et al., 1989; Pearson, 1995).

ODP Site 865 sits in an oceanographically dynamic area, relatively close to the edge of the guyot, where the sedimentary cap starts to thin, e.g., it lacks the thick Miocene-Quaternary overburden of the guyot centre (Shipboard Scientific Party, 1993a). The abraded appearance of reworked foraminifera (e.g., dull luster and fragmented) suggests that they have been exposed to intense mechanical erosion, e.g., from currents and/or a more intense transport history than the *in-situ* assemblage (Pilkey et al., 1969; Maikelm, 1967). Whereas the pervasive brown foraminiferal discoloration on many specimens, an oxidized iron stain, and pyrite likely reflect deposition in a low sedimentation (and hence high current intensity) area with iron sourced from the contemporaneous formation of manganese-phosphate hardgrounds or remobilized from the lower limestone platform. Together these lines of evidence suggest a similar reworking mechanism to that observed on other Pacific guyots (Pearson, 1995; Watkins et al., 1995) with sediments mobilized from the low sedimentation margins of the guyot top during discrete intervals of increased local current intensity, and temporarily mixed into sediments closer to the center of the pelagic cap. Crucially currents around Site 865 were clearly sufficient to mix and remobilize sediments at times in the late middle Eocene but not to scour the guyot top of sediments. Consistent with this hypothesis is a reduction of sedimentation rates above ~32 amcd (Figs 5 and S2) coincident with the zone of most intense reworking. Lower sedimentation rates, in addition to being consistent with elevated current activity either removing sediment or preventing deposition, would also reduce dilution of mixed components in sediments by *in-situ* fauna making the reworking more evident. Regardless of reworking, the ability to correlate the XRF records at the decimeter scale and the coherent stable isotope stratigraphy throughout Cores 865B-4H to -6H and 865C-4H to -6H suggests that if reworking is present it is relatively easy to avoid, not pervasive throughout the site, and most critically has not obscured primary environmental signals.

4.2 Climatic events at ODP Site 865

The long-term shift towards higher benthic foraminiferal $\delta^{18}O$ values observed through the Site 865 study interval (Fig. 5) is consistent with a previously published low-resolution benthic foraminiferal stable isotope record spanning the middle and upper Eocene at this site (Bralower et al., 1995; Coxall et al., 2000) as well as the global Eocene cooling trend (Bohaty and Zachos, 2003; Zachos et al., 2008). Superimposed on this long-term trend is a transient negative $\delta^{18}O$ excursion between ~35–36 amcd, within calcareous nannofossil and planktic foraminiferal Zones NP16 and E12, respectively, which is identified here as the MECO event (Fig. 5). The onset of the event is defined at the point where $\delta^{18}O$ begins to show a transition to lower values. The end of the event is less clearly defined, as at some other sites (Bohaty et al., 2009). However, the distinctive $\delta^{13}C$ maximum, which immediately follows the MECO (as in Bohaty et al., 2009) suggests that the abrupt increase in $\delta^{18}O$ values at 35 amcd likely marks the end of the event (see vertical yellow bar in Fig. 5). Indeed the gradual increase in $\delta^{18}O$ values that follows between ~30-35 amcd, is seen at ODP Sites 738 and 748 where the end of the event is clearly defined.

Our new XRF records allow us to create a composite record enabling us to capture the entire MECO event. However, very low sedimentation rates (<0.6 cm/kyr; Fig. 5 and Table S5) at this site compared to many other deep-sea sites (Bohaty and Zachos, 2003; Boscolo Galazzo et al., 2014; Edgar et al., 2010) mean that the event is highly condensed comprising a <1-m interval (Fig. 3). This is consistent with the reduced magnitude of the $\delta^{18}O$ excursion (~0.8‰ vs. 1.0-1.5‰) compared to elsewhere, the lack of a short (<50 kyr) negative $\delta^{13}C$ excursion coincident with peak MECO conditions (defined by the $\delta^{18}O$ minimum), and rapid apparent event onset (Boscolo Galazzo et al., 2014).

Because of its relatively shallow water sedimentation, Site 865 is a critical end-member for constraining the Pacific CCD response during the MECO and other Eocene shoaling events. Quantifying the amount, timing and pattern of CCD change across the MECO is essential to solving the so-called "carbon cycle conundrum" that the MECO currently poses (Sluijs et al., 2013). At >900 m, the CCD shoaling associated with the MECO is the largest known in the middle-to-late Eocene interval (shoaling from ~3.3-4.2 km paleowater depth; Pälike et al., 2012). Relatively continuous carbonate sedimentation across the event at ODP Site 865 suggests that the CCD did not shoal above ~1300–1500 m (the estimated paleowater depth of the site; Shipboard Scientific Party, 1993a) in the Pacific Ocean at this time providing a maximum limit of 3 km change.

The negative carbon and oxygen isotopic excursions represented here by only a single sample at ~ 43 amcd, in planktic foraminiferal Zone E11, immediately before a shift to more positive $\delta^{18}O$ values likely corresponds to the 'C19r event', a transient hyperthermal style event (<100 kyrs in duration) initially recognised at ODP Site 1260 in the equatorial Atlantic (Edgar et al., 2007). The C19r event is now also known from the South Atlantic at ODP Sites 1263 and 702 and referred to as the Late Lutetian Thermal Maximum (Westerhold et al., 2017). Similar to the MECO, the relatively small stable isotope excursions compared to elsewhere (0.4‰ and 0.2‰ vs. 1.5‰ and ~1.8‰, in $\delta^{13}C$ and $\delta^{18}O$ at ODP Sites 865 and 1260, respectively) are likely a function of the low sedimentation rates at this site (~0.4–0.6 cm/kyr vs. 2.0 cm/kyr at ODP Site 1260) compounded by lower sampling frequency and time averaging. This is the first record of the C19r event outside of the Atlantic Ocean and suggests that the C19r event is in fact global in nature and, as such, may be a valuable stratigraphic marker within the long >1 Myr planktic foraminiferal Zone E11 in which it falls.

A tentative astronomical tuning based on correlation of the band-pass filter of ln(Sr/Ca) to the 405-kyr component of eccentricity, anchoring the record near the onset of the MECO to the eccentricity minimum at 40.5 Ma (Westerhold and Röhl, 2013), is in close agreement with available biostratigraphic age control (Fig. 6). This interpretation places the peak $\delta^{18}O$ excursion during the MECO within a 405-kyr eccentricity maximum at 40.3 Ma, and the carbon-isotope maximum directly following the MECO coincides with the 405-kyr eccentricity minimum at 40.1 Ma, in agreement with Westerhold and Röhl (2013). The duration of the interval between the potential C19r event and the onset of the MECO is estimated at three and a half 405-kyr cycles or 1.4 Myr, which is longer than the duration estimated by Westerhold and Röhl (2013) at two and a half 405 kyr cycles, ~1 Myr. Unfortunately, a detailed comparison to existing cyclostratigraphic studies is hampered by uncertainty in the detection of the C19r event. The seemingly different duration estimate is in line with existing discrepancies between astrochronologies, notably in the reported length of magnetochron C19r, with duration estimates varying between 0.9 Myr (Westerhold and Röhl, 2013; Westerhold et al., 2015; Westerhold et al., 2014) and 1.5 Myr (Boulila et al., 2018).

4.3 Integrated biostratigraphic schemes and relationship to the MECO

Whilst both calcareous nannofossil and planktic foraminiferal zonation schemes can be applied to ODP Site 865 and are in generally good agreement, there is significant disagreement in the post-MECO interval between ~30 and 35 amcd (Fig. 6). Taken at face value, planktic foraminifera indicate constant sedimentation rates of ~0.5 cm/kyr throughout this interval whereas calcareous nannofossil datums suggest a 3.5 Myr hiatus between 38.6 and 42.1 Ma. However, XRF-derived elemental and stable isotope datasets and cyclostratigraphic analysis do not indicate any large shifts at this level that might indicate an abrupt shift in environmental conditions through time (Figs 2, 3 and

5). The presence of the MECO event itself, which falls within this potential gap, also implies that a hiatus is unlikely.

It is instead likely that low sedimentation rates and sampling frequency make it difficult to discern closely spaced calcareous nannofossil bioevents at Site 865, e.g., Tops of *C. solitus* and *S. furcatolithoides,* which are calibrated to a 130-kyr interval (40.40–40.53 Ma). However, these events also occur much higher in the section than expected relative to the MECO event at this site, and they also overlap with the much younger Top of *S. obtusus* and Base of *C. reticulatum* (Fig. 5). Explanations could include: these bioevents are diachronous and/or are not well calibrated or there is significant reworking of calcareous nannofossils. Indeed this interval does show evidence of reworking (Fig. 3), which could make the Tops of species appear higher in the section than expected and introduce a degree of subjectivity in determining what is *in situ* versus reworked, enhanced bioturbation and/or high core water content during this interval may have further affected the datum levels. However, a number of recent studies have questioned the accuracy of long-standing calcareous nannofossil age calibrations (e.g., Agnini et al., 2014; Tori and Monechi, 2013). For instance, many *Chiasmolithus* bioevents are no longer included in the newest calcareous nannofossil zonation scheme because typically low and sporadic abundances of these species at many sites introduces significant uncertainty to reported datum levels (Agnini et al., 2014; Larrasoaña et al., 2008; Villa et al., 2008). We also do see differences in the relative positions of the first occurrences of *D. bisectus* (<10μm) and *D. bisectus/scrippsae* (>10μm) in multiple studies, but this likely arises because of taxonomic ambiguity that has been associated with identifying these taxa (e.g., Backman, 1987; Larrasoaña et al., 2008; Mita, 2001; Tori and Monechi, 2013). The very high Base of *C. reticulatum* at the site is perhaps the most problematic, but reports of the position of this event from other sites are also variable, ranging from magnetochron C20r to C18n.2n (a ∼5 Myr interval; Fornaciari et al., 2010; Rivero-

Cuesta et al., 2019). However, given the sporadic and rare presence of *C. reticulatum* in our own observations here, the most likely explanation is ecological bias at Site 865. Similarly, *N. fulgens* is typically rare with an infrequent distribution at Site 865 and elsewhere, reducing its biostratigraphic utility (Bown, 2005; Shamrock, 2010).

The Base of *O. beckmanni* is diachronous, with the species first appearing in the tropics prior to the MECO but subsequently expanding to higher latitudes across the onset of the MECO and inferred surface water warming (Edgar et al., 2010; Jovane et al., 2010; Luciani et al., 2010). At Site 865, the Base of *O. beckmanni* precedes the MECO event consistent with this hypothesis (Fig. 3). The Top of *O. beckmanni* occurs after the MECO event at Site 865, as at ODP Site 1051 and in the Alano section in the Atlantic and Tethyan Oceans, respectively (Edgar et al., 2010; Luciani et al., 2010), suggesting that cooling of surface waters following the MECO was not directly responsible for its extinction. Regardless, planktic foraminiferal Zone E12 is a good marker for the MECO interval in (sub)tropical sediments that lack a stable isotope stratigraphy. The first occurrence of *D. scrippsae* (= *D. bisectus* <10 μm) at low- and mid-latitude sites is also used to approximate the beginning of the MECO event based on close correlation at a number of sites in the Atlantic Ocean (Bohaty et al., 2009). The Base of *D. bisectus* <10 μm does occur within the MECO event at ODP Site 865 (Fig. 5).

The robust and cosmopolitan planktic foraminifera *A. bullbrooki* is a valuable secondary marker close to the base of Zone E12 at 40.04 Ma (Gradstein et al., 2012; Wade et al., 2011) when *O. beckmanni* is absent either due to its relatively high susceptibility to mechanical damage and dissolution or limited (sub)tropical distribution (Edgar et al., 2010). However, here we find that the Top of *A. bullbrooki* and the Base of *O. beckmanni* are not synchronous as implied by the current biozonation scheme (Wade et al., 2011). Whilst there can be a degree of subjectivity in the definition of *O. beckmanni* between workers at the start of its range (Premoli Silva et al., 2006) this is not the case at ODP Site 865 where highly spherical and distinctive forms are present in the lowermost samples (assuming that downhole contamination is not a major issue; Fig. 4). There are relatively few sites where both taxa are reported but at ODP Sites 1051 and 1260, in the (sub)tropical Atlantic Ocean, the Top of *A. bullbrooki* also occurs significantly higher than the Base of *O. beckmanni* before (Site 1051) or even after the MECO event (Site 1260) (Edgar et al., 2010; Shipboard Scientific Party, 1998, 2004). In the Contessa section, Italy the Top of *A. bullbrooki* occurs significantly below the Base of *O. beckmanni* and the MECO (Jovane et al., 2010). Either way, the events are not contemporaneous suggesting that a significant revision of this datum is required.

Whilst *Hantkenina* is present in low abundance throughout the mid-late Eocene of Site 865 (Coxall et al., 2000), the transient appearance of rare *Hantkenina australis*, a distinctive middle Eocene form with recurved tubulospines, is present at Site 865 within the inferred C19r 'hyperthermal' event. This is surprising because this taxon is found globally, but, unlike most other *Hantkenina* spp., is most abundant at higher latitudes and, thus, in cooler waters (Coxall and Pearson, 2006). The appearance of *Hantkenina australis* may prove to be a future useful marker for C19r, an otherwise 'datum poor' interval. Notably, previous transient incursions of more tropical species of *Hantkenina* to high northern latitudes (>50°N) in the middle Eocene at ODP Site 647 has previously been used to infer surface ocean warming around the C19r interval (Shipboard Scientific Party, 1987). However, stratigraphic revision of ODP Site 647 by Firth et al. (2012) places the lower *Hantkenina* incursion at the base of calcareous nannofossil Zone NP16 and close to the Magnetochron 18r/19n boundary, which is significantly later than the C19r event but before the MECO – and inconsistent with the hypothesis of expansion of the *Hantkenina* range in response to warming surface waters. Thus, instead may reflect changes in upwelling or increased primary production (Coxall et al., 2007).

The top of *G. nuttalli* was introduced as the marker for the base of planktic foraminiferal Zone E11 in 2005, based on correlations at ODP Site 1050 and 1051 (R.D. Norris cited inBerggren and Pearson, 2005) to break up the otherwise very long multi-million year Zone P12 from the earlier zonation scheme (Berggren et al., 1995). However, occurrences of *G. nuttalli* (albeit small individuals) have now been found as high as Zone E14 (i.e., above the MECO) in the Alano section in northern Italy with the highest consistent occurrence in Zone E13 (Agnini et al., 2011). The datum level reported in Table 5 (XX amcd) is the highest consistent occurrence of this taxon at Site 865, but, similar to Alano, we do find at least sporadic occurrences of small individuals up through Zones E13 and E14 that are not obviously reworked.

A number of bioevents within Zone E10 at Site 865 are out of sequence with respect to the primary datum – the Top of *M. aragonensis* (43.26 Ma) - occurring above the Bases of younger taxa *G. index* and *M. lehneri* (at 42.64 and 43.15 Ma, respectively*)*. It is the highest occurrences of taxa that are most likely to be impacted by reworking. Yet *M. aragonensis* specimens do not show distinctive staining or worn appearance at this level (as they do higher up in Hole 865C where they are clearly reworked), and, whilst individuals could be remobilized locally, a higher Top of *M. aragonensis* compared to *G. index* is also evident in the Contessa section, Italy (Jovane et al., 2010).

Clearly more work is needed to confidently understand the relative patterns of calcareous nannofossil and planktic foraminiferal datums in the middle Eocene, particularly from the Pacific Ocean since most (if not all) calibrations are currently based on Atlantic or Tethyan sediment sequences and indeed few sites where both groups are inter-calibrated (e.g., Agnini et al., 2014; Berggren and Pearson, 2005). Whilst many key tropical middle Eocene bioevents are identified at Site 865, the lack of magnetic or confident astrochronology hinders determination of the absolute age of the events reported here. However, in the future, the high-resolution stable isotope and XRF records should enable the development of a more robust orbitally tuned age model here or allow correlation to sites elsewhere that do possess an independent reliable stratigraphy.

5. Conclusions

In this study, we have developed new biostratigraphic, stable isotope, and XRF records that span the MECO event at ODP Site 865 in the tropical Pacific Ocean. This site possesses a surprisingly pronounced signal in XRF-derived elemental counts and ratios permitting us to construct a reliable composite section for Holes 865B and 865C that spans the late middle Eocene time interval (~38–43 Ma). Cyclicity observed in XRF datasets is likely orbitally paced, and a tentative astronomical tuning of the study section indicates consistently low sedimentation rates of ~0.4-0.6 cm/kyr, in agreement bio- and chemostratigraphic age calibrations and correlations to other sites. Benthic foraminiferal stable isotope data indicate that the MECO and the C19r events are present at Site 865, albeit relatively condensed. Planktic foraminiferal biostratigraphic events from the classic zonation schemes are recognized here and are generally in good agreement with calibrated stratigraphies, with the exception of anomalously high occurrences of *G. nuttalli, A. bullbrooki* and *M. aragonensis*. When considered alongside available calcareous nannofossil datums, there is some disagreement in terms of both the relative ordering and position of calcareous microfossil events, particular with respect to the MECO event, which, in the absence of an independent age model, acts as a key stratigraphic marker. Thus, further calibrations of these bioevents are necessary, particularly from the Pacific Ocean, which is poorly represented in current calibration schemes. Microfossil reworking is also evident in the topmost ~30 m of Site 865, indicating a dynamic local hydrography capable of remobilizing and mixing sediments during the middle Eocene. ODP Site 865 is the first tropical record where the apparent entirety of the MECO event is preserved in carbonate bearing sediments, and, despite the reworking at this site, the primary environmental signals are preserved. Thus, ODP Site 865 represents a valuable site for future investigations into environmental and biotic change in the tropics during the MECO.

Data Availability

All raw data files are available in the supplement.

Author Contribution

KME conceived and coordinated the study, processed and analysed the samples for stable isotope analysis and developed a revised planktic foraminiferal biostratigraphy, drafted figures, and wrote the article; SMB carried out XRF analyses and constructed the mcd and amcd scales, SB conducted spectral analysis, constructed the orbital stratigraphy and drafted associated figures; PB conducted new calcareous nannofossil analyses, PNP and HKC contributed to the planktic foraminiferal biostratigraphy and taxonomy; CL supported the stable isotope work. All authors contributed to the writing and editing of the article.

Competing Interests

The authors declare that they have no conflict of interest.

Acknowledgements

This research used samples provided by the International Ocean Discovery Program (IODP). The authors would like to thank Sandra Nederbragt for technical assistance with $\delta^{18}O$ and $\delta^{13}C$ analyses and Cardiff University undergraduate students Bo Fan Peng, Jonathon Gamble and Holly Welsby for help picking benthic foraminifera. Financial support to KME was provided in the form of NERC grants (NE/H016457/1 and NE/P013112/1), and a Leverhulme Early Career Fellowship (ECF-2013-608).

Figure 1 – Location map for ODP Site 865 (solid star) and other low latitude sites discussed in the main text (open stars) on a 40 Ma reconstruction. Paleolatitudes for each site are calculated from van Hinsbergen et al. (2015).

Figure 2 – Sr/Ca and Ba/Sr records from ODP Holes 865B and 865C on the new adjusted metres composite depth (amcd) scale. The in-splice intervals are indicated by the horizontal bars at the bottom of the figure.

Figure 3 – Time series analyses of the ln(Sr/Ca) and Fe intensity data and tentative orbital tuning. From left to right: the La2011 eccentricity solution (dark blue) and its 405 kyr bandpass filter (light blue) and the ln(Sr/Ca) record and the Fe intensity record flanked by their 1.9 m (black) and 50 cm (grey) bandpass filters and evolutive power spectra, with e1, e2 and e3 indicating the potential imprint of the 405, 125 and 95 kyr components of eccentricity, respectively. The evolutive spectra are topped by redfit power spectra with dashed lines showing the 99, 95, 90 and 80% confidence levels and with main periodicities indicated. Horizontal yellow bands indicate the position of the MECO and the C19r event. Horizontal grey dashed lines indicate tentative tuning tie-points between the ln(Sr/Ca) bandpass filter and the astronomical solution.

Figure 4 - Scanning electron and light microscope images of biostratigraphically important taxa at ODP Site 865. (a and b) Sample ODP Hole 865C-4H-2, 25-27 cm, *Morozovelloides lehneri* – reworked specimens with distinctive brown/orange discoloration*;* (c and d) Sample ODP Hole 865C-4H-2, 85-87 cm, *Globigerinatheka*

semiinvoluta; (e) Sample ODP Hole 865C-5H-1, 5-7 cm, *Orbulinoides beckmanni*; (f) Sample ODP Hole 865C-5H-4, 85-87 cm, *Acarinina bullbrooki*; (g) Sample ODP Hole 865C-4H-3, 95-97 cm, a reworked *Morozovella aragonensis*; (h) Sample ODP Hole 865C-5H-2, 45-47 cm, *Globigerinatheka index*; (i) Sample ODP Hole 865C-5H-2, 45-47 cm, *Morozovelloides lehneri*. All scale bars are 100 μm.

Figure 5 – Benthic foraminiferal stable isotope records and age control points in ODP Holes 865B and 865C. (a and b) $\delta^{18}O$ and $\delta^{13}C$ values are from multi-specimen analyses of *Nuttallides truempyi* (no vital effect correction has been applied). Gaps in the records represent intervals where no data was generated. (c) Planktic foraminiferal datums are from this study (Table 5). (d) Nannofossil biostratigraphic markers are from Bralower and Mutterlose (1995) with new data here (Table 6). Depth uncertainty on datums are indicated by vertical lines (black lines = amcd scale; grey line = top or bottom depth falls outside of amcd scale and is shown on mbsf) and where not visible are smaller than the symbol. (e) Sedimentation rates on amcd scale based on orbital tuning tie-points (Supplementary Table 4) The vertical yellow bars define the positions of the Middle Eocene climatic optimum (MECO) and the possible C19r event. T = top; B= base; Bc = base of common occurrence. Note that only datums that fall within the new amcd scale are shown here.

Figure 6 – Age–depth plot for ODP Site 865. Only datums falling within the new adjusted meters composite depth (amcd) scale are included here. To see all calcareous microfossil datums from the study interval see Supplementary Figure 2. Planktic foraminiferal datums are from this study and H. Coxall *unpub*. (presented in Pearson and Ezard (2014)) (Table 5). Calcareous nannofossil datums are from this study and Bralower and Mutterlose (1995) (Table 6). Depth uncertainty on datums are indicated by vertical lines (black lines = amcd scale; grey line = top or bottom depth falls outside

of amcd scale and is shown on mbsf) and where not visible are smaller than the symbol. Black diamonds are the tuning tie-points to the orbital solution (Supplementary Table 4). Ages are shown on the Gradstein et al. (2012) timescale. amcd = adjusted metres composite depth. Abbreviations of datums are T or B for Top or Base followed by the first letter of the genus and species name.

Table 1 – Composite depth offsets within splice for ODP Site 865.

Table 2 - Splice tie-points for ODP Site 865.

Table 3 – Mapping pairs for adjusting mcd to amcd for ODP Hole 865B.

Table 4 – Mapping pairs for adjusting mcd to amcd for ODP Hole 865C.

Table 5 – Planktic foraminiferal datums in ODP Holes 865B and C.

Table 6 – Calcareous nannofossil datums in ODP Holes 865B and C.

Supplementary Figure 1. Sedimentation rate estimate using the ASM method, applied to the Fe intensity records from 32.5 to 44.5 m. The lowermost panel shows MTM analyses of the data with confidence levels indicated. Vertical dashed bars indicate periodicities detected above the 90% confidence level, that are compared to the periodicities of long eccentricity at 405 kyr (E1), short eccentricity at 125 kyr (E2) and 95 kyr (E3), obliquity at 39.2 kyr (O) and precession at 23.1 (P1) and 21.8 (P2) kyr . The sedimentation rates at which the optimal fit is achieved are indicated in the topmost panels. The middle panels show that the significance level threshold (dashed line) is passed, so that the null hypothesis of no orbital forcing can be rejected.

Supplementary Figure 2. Age depth plot for ODP Site 865 on metres below seafloor (mbsf) depth scale to assess degree of offset between cores pre-alignment (and new amcd scale). Planktic foraminiferal datums are from this study and H. Coxall *unpub*. (presented in Pearson and Ezard (2014)) (Table 5). Calcareous nannofossil datums are from this study and Bralower and Mutterlose (1995) (Table 6). Depth uncertainty on datums are indicated by vertical lines and where not visible are smaller than the symbol. Ages are shown on the Gradstein et al. (2012) timescale. amcd = adjusted metres composite depth.

Supplementary Table 1: Raw elemental intensity counts for ODP Holes 865B and 865C – (Too big to upload need to put in doi)

Supplementary Table 2: Benthic foraminifer (*Nuttallides truempyi*) stable isotope analyses for ODP Hole 865B

Supplementary Table 3: Benthic foraminifer (*Nuttallides truempyi*) stable isotope analyses for ODP Hole 865C

Supplementary Table 4: Tuning tie-points on adjusted' metres composite depth (amcd).

6. References

Agnini, C., Fornaciari, E., Giusberti, L., Grandesso, P., Lanci, L., Luciani, V., Muttoni, G., Paelike, H., Rio, D., Spofforth, D.J.A., Stefani, C., 2011. Integrated biomagnetostratigraphy of the Alano section (NE Italy): A proposal for defining the middle-late Eocene boundary. Geological Society of America Bulletin 123, 841-U110.

Agnini, C., Fornaciari, E., Raffi, I., Catanzariti, R., Pälike, H., Backman, J., Rio, D., 2014. Biozonation and biochronology of Paleogene calcareous nannofossils from low and middle latitudes. Newsletters on Stratigraphy 47, 131-181.

Arreguín-Rodríguez, G.J., Alegret, L., Thomas, E., 2016a. Late Paleocene-middle Eocene benthic foraminifera on a Pacific seamount (Allison Guyot, ODP Site 865): Greenhouse climate and superimposed hyperthermal events. Paleoceanography 31, 346-364.

Arreguín-Rodríguez, G.J., Alegret, L., Thomas, E., 2016b. Late Paleocene-middle Eocene benthic foraminifera on a Pacific seamount (Allison Guyot, ODP Site 865): Greenhouse climate and superimposed hyperthermal events. Paleoceanography, n/a-n/a.

Backman, J., 1987. Quantitative calcareous nannofossil biochronology of middle Eocene through early Oligocene sediment from DSDP Sites 522 and 523. Abh. Geol. B.-A 39, 21-31.
Berggren, W.A., Kent, D.V., Swisher III, C.C., Aubry, M.-P., 1995. A revised Cenozoic geochronology and chronostratigraphy, Geochronology Time Scales and Global Stratigraphci Correlation Special Publication. Society for Sedimentary Geology (SEPM).
Berggren, W.A., Pearson, P.N., 2005. A Revised Tropical to Subtropical Paleogene Planktonic Foraminiferal Zonation. The Journal of Foraminiferal Research 35, 279-298.
Bijl, P.K., Houben, A.J.P., Schouten, S., Bohaty, S.M., Sluijs, A., Reichart, G.-J., Sinninghe Damsté, J.S., Brinkhuis, H., 2010. Transient Middle Eocene Atmospheric CO2 and Temperature Variations. Science 330, 819-821.
Bohaty, S.M., Zachos, J.C., 2003. Significant Southern Ocean warming event in the late middle Eocene. Geology 31, 1017-1020.
Bohaty, S.M., Zachos, J.C., Florindo, F., Delaney, M.L., 2009. Coupled greenhouse warming and deep-sea acidification in the middle Eocene. Paleoceanography 24, PA2207.
Boscolo Galazzo, F., Thomas, E., Giusberti, L., 2015. Benthic foraminiferal response to the Middle Eocene Climatic Optimum (MECO) in the South-Eastern Atlantic (ODP Site 1263). Palaeogeography, Palaeoclimatology, Palaeoecology, 432-444.
Boscolo Galazzo, F., Thomas, E., Pagani, M., Warren, C., Luciani, V., Giusberti, L., 2014. The middle Eocene climatic optimum (MECO): A multiproxy record of paleoceanographic changes in the southeast Atlantic (ODP Site 1263, Walvis Ridge). Paleoceanography, 2014PA002670.
Boulila, S., Vahlenkamp, M., De Vleeschouwer, D., Laskar, J., Yamamoto, Y., Pälike, H., Kirtland Turner, S., Sexton, P., Westerhold, T., Röhl, U., 2018. Towards a robust and consistent middle Eocene astronomical timescale. Earth and Planetary Science Letters 486, 94-107.
Bown, P., 2005. Palaeogene calcareous nannofossils from the Kilwa and Lindi areas of coastal Tanzania (Tanzania Drilling Project Sites 1 to 10, 2003-4). Journal of Nannoplankton Research 27, 21-95.
Bralower, T.J., Mutterlose, J., 1995. Calcareous nannofossil biostratigraphy of Site 865, Allison Guyot, central Pacific Ocean: A tropical Paleogene reference section, Proceedings of the Ocean Drilling Program, Scientific Results. Ocean Drilling Program, College Station Tex, pp. 31-74.
Bralower, T.J., Zachos, J.C., Thomas, E., Parrow, M., Paull, C.K., Kelly, D.C., Silva, I.P., Sliter, W.V., Lohmann, K.C., 1995. Late Paleocene to Eocene paleoceanography of the equatorial Pacific Ocean: Stable isotopes recorded at Ocean Drilling Program Site 865, Allison Guyot. Paleoceanography 10, 841-865.
Coxall, H.K., Pearson, P.N., 2006. Taxonomy, biostratigraphy, and phylogeny of the Hantkeninidae (Clavigerinella, Hantkenina, and Cribrohantkenina). Cushman Foundation for Foraminiferal Research Special Publication 41, 213-256.
Coxall, H.K., Pearson, P.N., Shackleton, N.J., Hall, M.A., 2000. Hantkeninid depth adaptation: An evolving life strategy in a changing ocean. Geology 28, 87-90.
Coxall, H.K., Wilson, P.A., Pearson, P.N., Sexton, P.F., 2007. Iterative evolution of digitate planktonic foraminifera. Paleobiology 33, 495-516.

Cramwinckel, M.J., van der Ploeg, R., Bijl, P.K., Peterse, F., Bohaty, S., Röhl, U., Schouten, S., Middleburg, J., Sluijs, A., 2019. Harmful algae and export production collapse in the equatorial Atlantic during the zenith of Middle Eocene Climatic Optimum warmth. Geology 47, 247-250.

Dawber, C.F., Tripati, A.K., 2011. Constraints on glaciation in the middle Eocene (46–37 Ma) from Ocean Drilling Program (ODP) Site 1209 in the tropical Pacific Ocean. Paleoceanography 26.

Dutton, A., Lohmann, K.C., Leckie, R.M., 2005. Insights from the Paleogene tropical Pacific: Foraminiferal stable isotope and elemental results from Site 1209, Shatsky Rise. Paleoceanography 20.

Edgar, K.M., Anagnostou, E., Pearson, P.N., Foster, G.L., 2015. Assessing the impact of diagenesis on δ11B, δ13C, δ18O, Sr/Ca and B/Ca values in fossil planktic foraminiferal calcite. Geochimica et Cosmochimica Acta 166, 189-209.

Edgar, K.M., Bohaty, S.M., Gibbs, S.J., Sexton, P.F., Norris, R.D., Wilson, P.A., 2013. Symbiont 'bleaching' in planktic foraminifera during the Middle Eocene Climatic Optimum. Geology 41, 15-18.

Edgar, K.M., Wilson, P.A., Sexton, P.F., Gibbs, S.J., Roberts, A.P., Norris, R.D., 2010. New biostratigraphic, magnetostratigraphic and isotopic insights into the Middle Eocene Climatic Optimum in low latitudes. Palaeogeogr Palaeocl 297, 670-682.

Edgar, K.M., Wilson, P.A., Sexton, P.F., Suganuma, Y., 2007. No extreme bipolar glaciation during the main Eocene calcite compensation shift. Nature 448, 908-911.

Expedition 320/321 Scientists, 2009. Site U1333, in: Palike, H., Lyle, M., Nishi, H., Raffi, I., Gamage, K., Klaus, A. (Eds.), Proceedings of the Integrated Ocean Drilling Program. Integrated Ocean Drilling Program Management International, Inc., Texas A&M University.

Firth, J.V., Eldrett, J.S., Harding, I.C., Coxall, H.K., Wade, B.S., 2012. Integrated biomagnetochronology for the Palaeogene of ODP Hole 647A: implications for correlating palaeoceanographic events from high to low latitudes. Geological Society, London, Special Publications 373.

Fornaciari, E., Agnini, C., Catanzariti, R., Rio, D., Bolla, E.M., Valvasoni, E., 2010. Mid-latitude calcareous nannofossil biostratigraphy and biochronology across the middle to late Eocene transition. Stratigraphy 7, 229-264.

Genin, A., Noble, M., Lonsdale, P.F., 1989. Tidal currents and anticyclonic motions on two North Pacific seamounts. Deep Sea Research Part A. Oceanographic Research Papers 36, 1803-1815.

Gradstein, F.M., Ogg, J.G., Schmitz, M., Ogg, G., 2012. The Geologic Time Scale 2012 2-Volume Set. Elsevier, Boston, USA.

Holbourn, A., Henderson, A.S., MacLeod, N., 2013. Atlas of benthic foraminifera. John Wiley & Sons.

Jovane, L., Florindo, F., Coccioni, R., Dinarès-Turell, J., Marsili, A., Monechi, S., Roberts, A.P., Sprovieri, M., 2007. The middle Eocene climatic optimum event in the Contessa Highway section, Umbrian Apennines, Italy. Geological Society of America Bulletin 119, 413-427.

Jovane, L., Sprovieri, M., Coccioni, R., Florindo, F., Marsili, A., Laskar, J., 2010. Astronomical calibration of the middle Eocene contessa Highway section (Gubbio, Italy). Earth and Planetary Science Letters 298, 77-88.

Kelly, C.D., Bralower, T.J., Zachos, J.C., Silva, I.P., Thomas, E., 1996. Rapid diversification of planktonic foraminifera in the tropical Pacific (ODP Site 865) during the late Paleocene thermal maximum. Geology 24, 423-426.

Kelly, D.C., Bralower, T.J., Zachos, J.C., 1998. Evolutionary consequences of the latest Paleocene thermal maximum for tropical planktonic foraminifera. Palaeogeography, Palaeoclimatology, Palaeoecology 141, 139-161.

Kozdon, R., Kelly, D.C., Kita, N.T., Fournelle, J.H., Valley, J.W., 2011. Planktonic foraminiferal oxygen isotope analysis by ion microprobe technique suggests warm tropical sea surface temperatures during the Early Paleogene. Paleoceanography 26, PA3206.

Kozdon, R., Kelly, D.C., Kitajima, K., Strickland, A., Fournelle, J.H., Valley, J.W., 2013. In situ δ 18O and Mg/Ca analyses of diagenetic and planktic foraminiferal calcite preserved in a deep-sea record of the Paleocene-Eocene thermal maximum. Paleoceanography 28, 517-528.

Larrasoaña, J.C., Gonzalvo, C., Molina, E., Monechi, S., Ortiz, S., Tori, F., Tosquella, J., 2008. Integrated magnetobiochronology of the Early/Middle Eocene transition at Agost (Spain): Implications for defining the Ypresian/Lutetian boundary stratotype. Lethaia 41, 395-415.

Laskar, J., Gastineau, M., Delise, J.-B., Farrés, A., Fienga, A., 2011. Strong chaos induced by close encounters with Ceres and Vesta. Astronomy and Astrophysics 532.

Luciani, V., Giusberti, L., Agnini, C., Fornaciari, E., Rio, D., Spofforth, D.J.A., Pälike, H., 2010. Ecological and evolutionary response of Tethyan planktonic foraminifera to the middle Eocene climatic optimum (MECO) from the Alano section (NE Italy). Palaeogeography, Palaeoclimatology, Palaeoecology 292, 82-95.

Martini, E., 1971. Standard Tertiary calcareous nannoplankton zonation, in: Farninacci, A. (Ed.), Proceedings of the II Plankton Conference Roma. Tecnoscienza, Rome.

Matthews, J.L., Heezen, B.C., Catalano, R., Coogan, A., Tharp, M., Natland, J., Rawson, M., 1974. Cretaceous Drowning of Reefs on Mid-Pacific and Japanese Guyots. Science 184, 462-464.

Meyers, S.R., 2014. Astrochron: An R Package for Astrochronology. .

Mita, I., 2001. Data Report: Early to late Eocene calcareous nannofossil assemblages of Sites 1051 and 1052, Blake Nose, North western Atlantic Ocean, in: Kroon, D., Norris, R.D., Klaus, A. (Eds.), Proceedings of the Ocean Drilling Program, Scientific Reports. Ocean Drilling Program, College Station, TX, pp. 1-28.

Möbius, I., Friedrich, O., Edgar, K.M., Sexton, P.F., 2015. Episodes of intensified biological productivity in the subtropical Atlantic Ocean during hte termination of the Middle Eocene Climatic Optimum. Paleoceanography.

Norris, R., Nishi, H., 2001. Evolutionary trends in coiling of tropical Paleogene planktic foraminifera. Paleobiology 27, 327-347.

Olsson, R.K., Pearson, P.N., Huber, B.T., 2006. Taxonomy, biostratigraphy and phylogeny of Eocene Catapsydrax, Globorotaloides, Guembelitrioides, Paragloborotalia, Parasubbotina, and Pseudoglobigerinella n. gen., in: Pearson, P.N., Olsson, R.K., Huber, B.T., Hemleben, C., Berggren, W.A., Coxall, H.K. (Eds.), Atlas of Eocene Planktonic Foraminifera, 1 ed. Cushman Foundation, Fredericksburg, USA, pp. 67-110.

Paillard, D., Labeyrie, L., Yiou, P., 1996. Macintosh Program performs time-series analysis. Eos, Transactions American Geophysical Union 77, 379-379.

Pälike, H., Lyle, M.W., Nishi, H., Raffi, I., Ridgwell, A., Gamage, K., Klaus, A., Acton, G., Anderson, L., Backman, J., Baldauf, J., Beltran, C., Bohaty, S.M., Bown, P., Busch, W., Channell, J.E.T., Chun, C.O.J., Delaney, M., Dewangan, P., Jones, T.D., Edgar, K.M., Evans, H., Fitch, P., Foster, G.L., Gussone, N., Hasegawa, H., Hathorne, E.C., Hayashi, H., Herrle, J.O., Holbourn, A., Hovan, S., Hyeong, K., Iijima, K., Ito, T., Kamikuri, S., Kimoto, K., Kuroda, J., Leon-Rodriguez, L., Malinverno, A., Moore, T.C., Murphy, B.H., Murphy, D.P., Nakamura, H., Ogane, K., Ohneiser, C., Richter, C., Robinson, R., Rohling, E.J., Romero, O., Sawada, K., Scher, H., Schneider, L., Sluijs, A., Takata, H., Tian, J., Tsujimoto, A., Wade, B.S., Westerhold, T., Wilkens, R., Williams, T., Wilson, P.A., Yamamoto, Y., Yamamoto, S., Yamazaki, T., Zeebe, R.E., 2012. A Cenozoic record of the equatorial Pacific carbonate compensation depth. Nature 488, 609-+.

Pearson, P., 1995. Planktonic foraminifer biostratigraphy and the development of pelagic caps on guyots in the Marshall Islands group, Proceedings of the Ocean Drilling Program. Scientific results. Ocean Drilling Program, pp. 21-59.

Pearson, P.N., Ditchfield, P.W., Singano, J., Harcourt-Brown, K.G., Nicholas, C.J., Olsson, R.K., Shackleton, N.J., Hall, M.A., 2001. Warm tropical sea surface temperatures in the Late Cretaceous and Eocene epochs. Nature 413, 481-487.

Pearson, P.N., Ezard, T.H.G., 2014. Evolution and speciation in the Eocene planktonic foraminifer Turborotalia. Paleobiology 40, 130-143.

Pearson, P.N., Olsson, R.K., Huber, B.T., Hemleben, C., Berggren, W.A., Coxall, H.K., 2006. Atlas of Eocene Planktonic Foraminifera. Cushman Foundation, Fredericksburg, USA.

Pearson, P.N., Palmer, M.R., 2000. Atmospheric carbon dioxide concentrations over the past 60 million years. Nature 406, 695-699.

Premoli Silva, I., Haggerty, J., Rack, F., Party, S.S., 1993. Proceedings of the Ocean Drilling Program Initial Reports. Ocean Drilling Program, College Station, Texas.

Premoli Silva, I., Wade, B.S., Pearson, P.N., 2006. TAXONOMY, BIOSTRATIGRAPHY, AND PHYLOGENY OF GLOBIGERINATHEKA AND ORBULINOIDES, in: Pearson, P.N., Olsson, R.K., Huber, B.T., Hemleben, C., Berggren, W.A. (Eds.), Atlas of Eocene Planktonic Foraminifera, 1 ed. Cushman Foundation Special Publication, pp. 169-212.

Rivero-Cuesta, L., Westerhold, T., Agnini, C., Dallanave, E., Wilkens, R.H., Alegret, L., Paleoenvironmental Changes at ODP Site 702 (South Atlantic): Anatomy of the Middle Eocene Climatic Optimum. Paleoceanography and Paleoclimatology n/a.

Rivero-Cuesta, L., Westerhold, T., Agnini, C., Dallanave, E., Wilkens, R.H., Alegret, L., 2019. Paleoenvironmental Changes at ODP Site 702 (South Atlantic): Anatomy of the Middle Eocene Climatic Optimum. Paleoceanography and Paleoclimatology 34, 2047-2066.

Röhl, U., Abrams, L.J., 2000. High resolution, downhole, and nondestructive core measurements from sites 999 and 1001 in the Caribbean Sea: Application to the late Paleocene thermal maximum, in: Leckie, R.M., Sigurdsson, H., Acton, G.D., Draper, G. (Eds.), Proceedings of the Ocean Drilling Program, Scientific Results, College Station, TX, pp. 191-203.

Savian, J., Jovane, L., Trindade, R., Frontalini, F., Coccioni, R., Bohaty, S., Wilson, P., Florindo, F., Roberts, A., 2013. Middle Eocene Climatic Optimum (MECO) in the Monte Cagenero section, central Italy. Latinmag Letters 3.

Schulz, M., Mudelsee, M., 2002. REDFIT: estimating red-noise spectra directly from unevenly spaced paleoclimatic time series. Computers & Geosciences 28, 421-426.

Sexton, P.F., Norris, R.D., Wilson, P.A., Palike, H., Westerhold, T., Rohl, U., Bolton, C.T., Gibbs, S., 2011. Eocene global warming events driven by ventilation of oceanic dissolved organic carbon. Nature 471, 349-352.

Sexton, P.F., Wilson, P.A., Pearson, P.N., 2006. Microstructural and geochemical perspectives on planktic foraminiferal preservation: "Glassy'' versus "Frosty''. Geochemistry Geophysics Geosystems 7.

Shamrock, J.L., 2010. A new calcareous nannofossil species of the genus Sphenolithus from the Middle Eocene (Lutetian) and its biostratigraphic significance. Journal of Nannoplankton Research 31, 5-10.

Shipboard Scientific Party, 1987. Site 647, in: Srivastava, S.P., Arthur, M.A., Clement, B. (Eds.), Proceedings of the Ocean Drilling Program, Initial Reports. Ocean Drilling Program, Texas A&M University.

Shipboard Scientific Party, 1993a. Site 865, in: Sager, W.W., Winterer, E.L., Firth, J.V., Party, S.S. (Eds.), Proceedings of the Ocean Drilling Program, Initial Reports 143. Ocean Drilling Program, College Station, TX pp. 111-180.

Shipboard Scientific Party, 1993b. Synthesis of Results, Leg 143, in: Sager, W.W., Winterer, E.L., Firth, J.V., Party, S.S. (Eds.), Proceedings of the Ocean Drilling Program, Initial Reports 143. Ocean Drilling Program, College Station, TX

Shipboard Scientific Party, 1998. Site 1051, in: Norris, R.D., Kroon, D., Klaus, A., Party, S.S. (Eds.), Proceedings of the Ocean Drilling Program, Initial Reports. Ocean Drilling Program, College Station, TX.

Shipboard Scientific Party, 2002. Site 1209, in: Bralower, T.J., Premoli-Silva, I., Malone, M.J., Shipboard Scientific Party (Eds.), Proceedings Ocean Drilling Project Initial Reports. Ocean Drilling Program, College Station, TX, pp. 1-102.

Shipboard Scientific Party, 2004. Site 1260, in: Erbacher, J., Mosher, D.C., Malone, M.J., Party, S.S. (Eds.), Proceedings of the Ocean Driling Project Initial Reports. Ocean Drilling Program, College Station, TX, pp. 1-113.

Spofforth, D.J.A., Agnini, C., Pälike, H., Rio, D., Fornaciari, E., Giusberti, L., Luciani, V., Lanci, L., Muttoni, G., 2010. Organic carbon burial following the middle Eocene climatic optimum in the central western Tethys. Paleoceanography 25, PA3210.

Tori, F., Monechi, S., 2013. Lutetian calcareous nannofossil events in the Agost section (Spain): implications toward a revision of the Middle Eocene biomagnetostratigraphy. Lethaia 46, 293-307.

Tripati, A.K., Delaney, M.L., Zachos, J.C., Anderson, L.D., Kelly, D.C., Elderfield, H., 2003. Tropical sea ‐ surface temperature reconstruction for the early Paleogene using Mg/Ca ratios of planktonic foraminifera. Paleoceanography 18.

Tripati, A.K., Elderfield, H., 2004. Abrupt hydrographic changes in the equatorial Pacific and subtropical Atlantic from foraminiferal Mg/Ca indicate greenhouse origin for the thermal maximum at the Paleocene-Eocene Boundary. Geochemistry, Geophysics, Geosystems 5, Q02006.

van Hinsbergen, D.J.J., de Groot, L.V., van Schaik, J., Spakman, W., Bijl, P.K., Sluijs, A., Langereis, C.G., Brinkhuis, H., 2015. A Paleolatitude Calculator for Paleoclimate Studies. PLoS ONE 10.

Villa, G., Fioroni, C., Pea, L., Bohaty, S., Persico, D., 2008. Middle Eocene–late Oligocene climate variability: Calcareous nannofossil response at Kerguelen Plateau, Site 748. Mar Micropaleontol 69, 173-192.

Wade, B.S., Pearson, P.N., Berggren, W.A., Pälike, H., 2011. Review and revision of Cenozoic tropical planktonic foraminiferal biostratigraphy and calibration to the geomagnetic polarity and astronomical time scale. Earth-Science Reviews 104, 111-142.

Watkins, D.K., Pearson, P.N., Erba, E., Rack, F., Premoli Silva, I., Bohrmann, H.W., Fenner, J., Hobbs, P.N., 1995. Stratigraphy and Sediment Accumulation Patterns of the Upper Cenozoic Pelagic Carbonate Caps of Guyots in the Northwestern Pacific Ocean, in: Haggerty, J., Premoli Silva, I., Rack, F., McNutt, M.K. (Eds.), Proceedings of the Ocean Drilling Program Scientific Reports. Ocean Drilling Program, College Station, TX.

Westerhold, T., Röhl, U., 2013. Orbital pacing of Eocene climate during the Middle Eocene Climate Optimum and the chron C19r event: Missing link found in the tropical western Atlantic. Geochemistry, Geophysics, Geosystems 14, 4811-4825.

Westerhold, T., Röhl, U., Donner, B., Frederichs, T., Kordesch, W.E.C., Bohaty, S.M., Hodell, D.A., Laskar, J., Zeebe, R.E., Late Lutetian Thermal Maximum—Crossing a Thermal Threshold in Earth's Climate System? Geochemistry, Geophysics, Geosystems, n/a-n/a.

Westerhold, T., Röhl, U., Donner, B., Frederichs, T., Kordesch, W.E.C., Bohaty, S.M., Hodell, D.A., Laskar, J., Zeebe, R.E., 2017. Late Lutetian Thermal Maximum—Crossing a Thermal Threshold in Earth's Climate System? Geochemistry, Geophysics, Geosystems 19.

Westerhold, T., Röhl, U., Frederichs, T., Bohaty, S.M., Zachos, J.C., 2015. Astronomical calibration of the geological timescale: closing the middle Eocene gap. Clim. Past 11, 1181-1195.

Westerhold, T., Röhl, U., Pälike, H., Wilkens, R., Wilson, P.A., Acton, G., 2014. Orbitally tuned timescale and astronomical forcing in the middle Eocene to early Oligocene. Clim. Past 10, 955-973.

Witkowski, J., Bohaty, S.M., Edgar, K.M., Harwood, D.M., 2014. Rapid fluctuations in mid-latitude siliceous plankton production during the Middle Eocene Climatic Optimum (ODP Site 1051, western North Atlantic). Mar Micropaleontol 106, 110-129.

Zachos, J.C., Dickens, G.R., Zeebe, R.E., 2008. An early Cenozoic perspective on greenhouse warming and carbon-cycle dynamics. Nature 451, 279.

Edgaretal_Figure 1

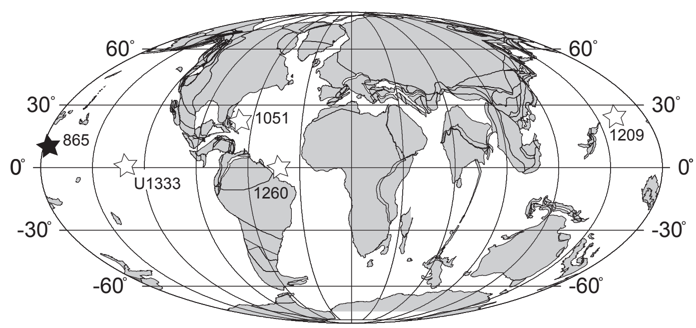

Edgar_Figure 2

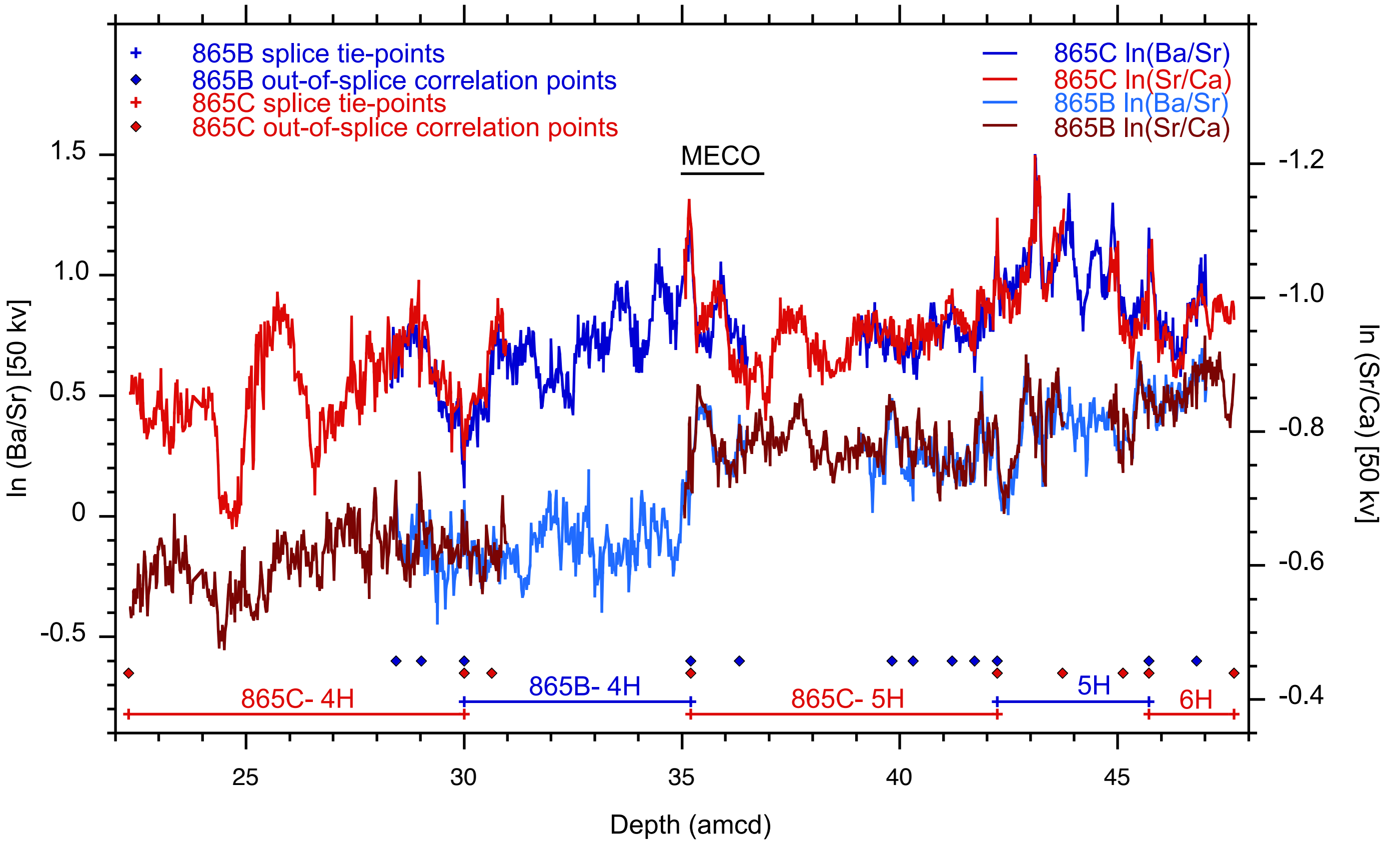

Edgar_Figure 3

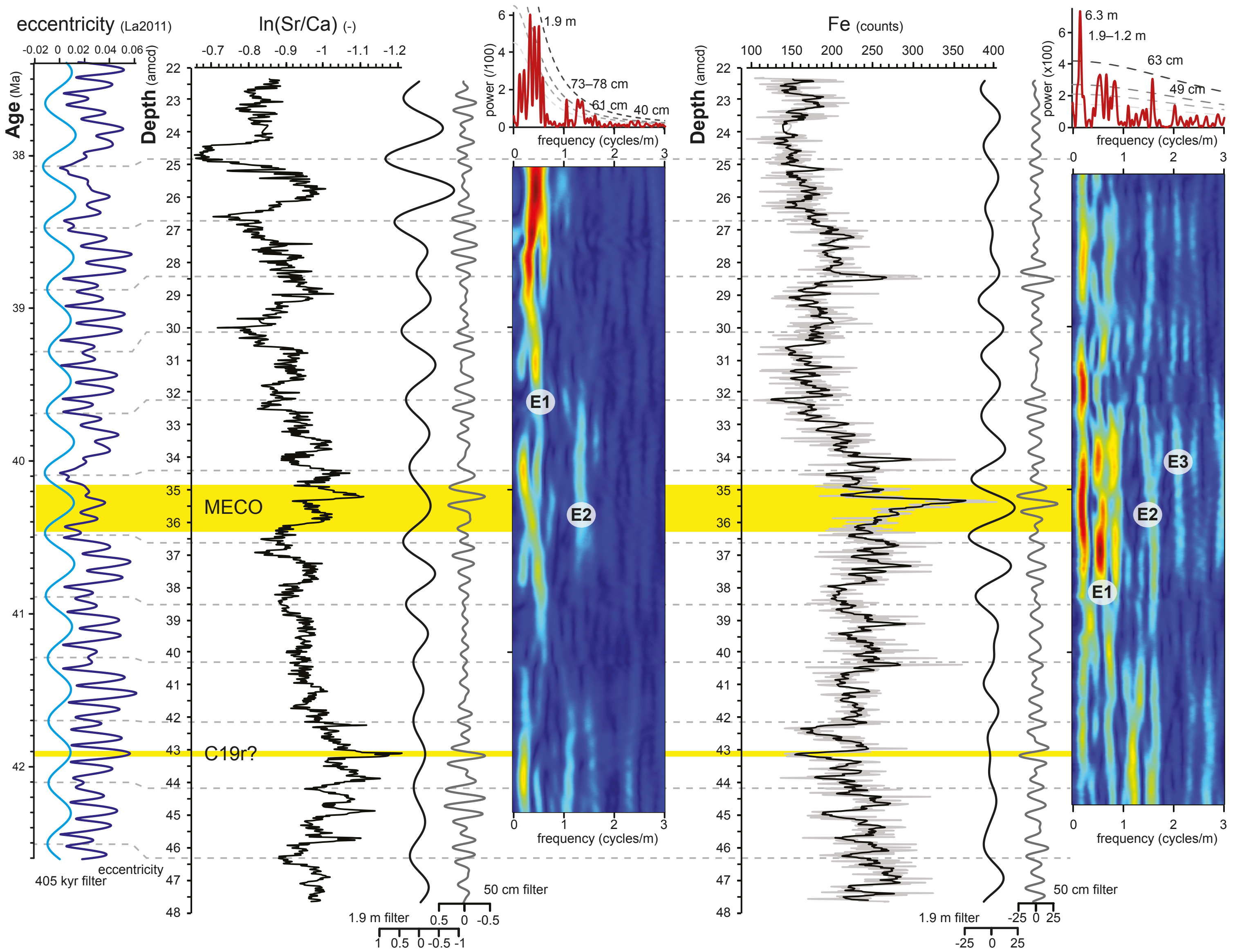

Edgar_Figure4

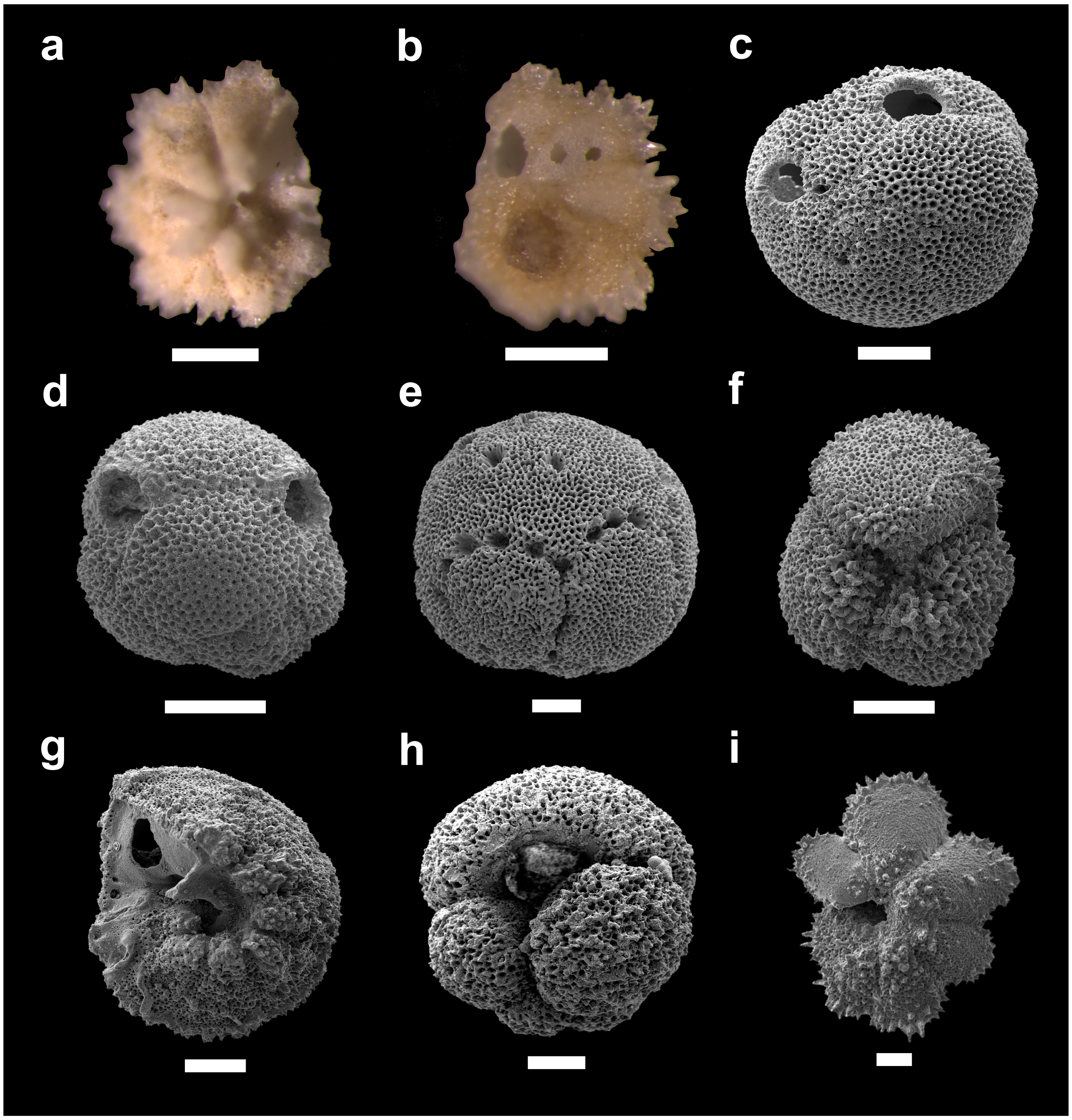

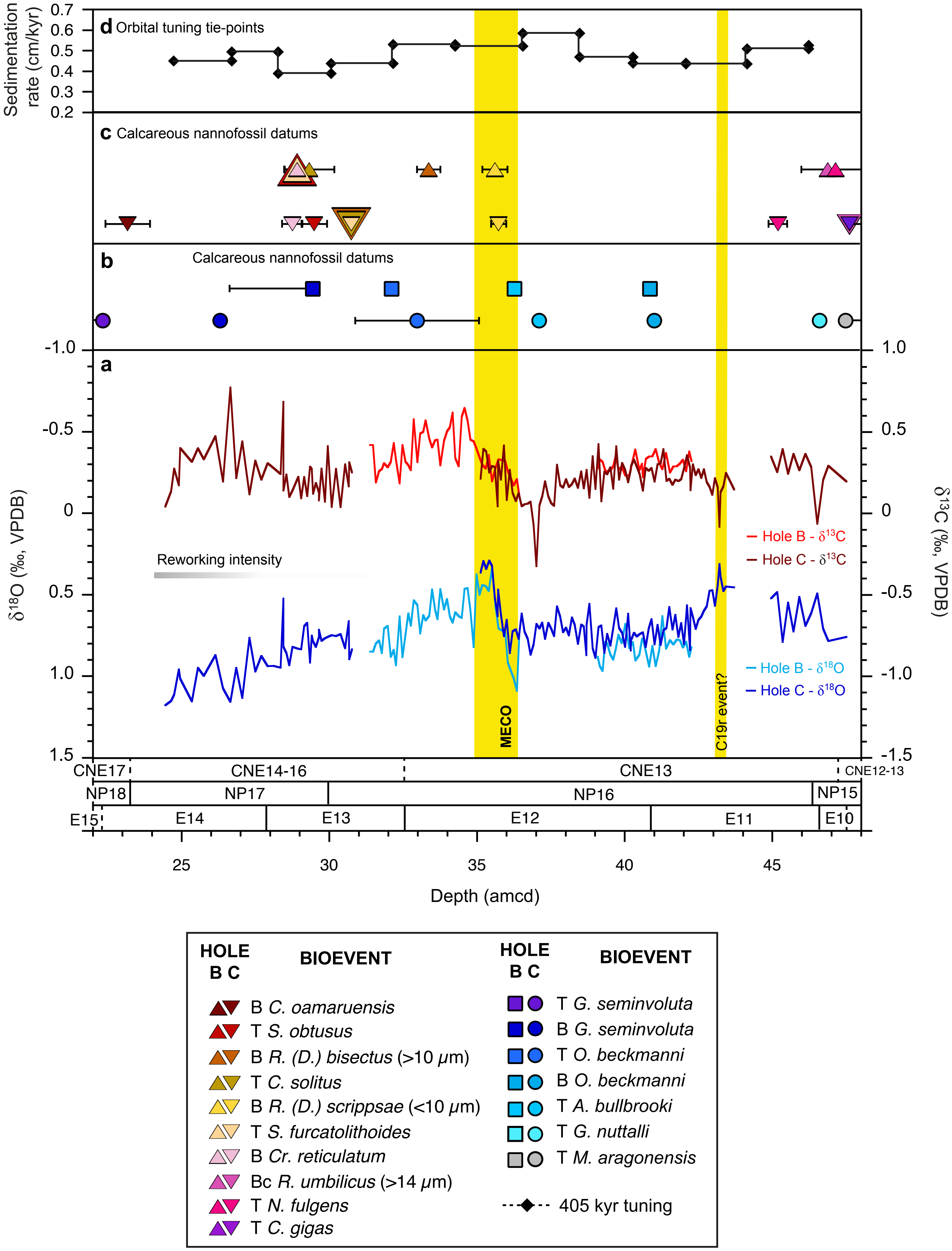

d Orbital tuning tie-points
Sedimentation rate (cm/kyr)
c Calcareous nannofossil datums
b Calcareous nannofossil datums
a
Reworking intensity
MECO
C19r event?
δ18O (‰, VPDB)
δ13C (‰, VPDB)
Hole B - δ13C
Hole C - δ13C
Hole B - δ18O
Hole C - δ18O
CNE17
CNE14-16
CNE13
CNE12-13
NP18
NP17
NP16
NP15
E15
E14
E13
E12
E11
E10
Depth (amcd)
HOLE B C
BIOEVENT
B C. oamaruensis
T S. obtusus
B R. (D.) bisectus (>10 μm)
T C. solitus
B R. (D.) scrippsae (<10 μm)
T S. furcatolithoides
B Cr. reticulatum
Bc R. umbilicus (>14 μm)
T N. fulgens
T C. gigas
T G. seminvoluta
B G. seminvoluta
T O. beckmanni
B O. beckmanni
T A. bullbrooki
T G. nuttalli
T M. aragonensis
405 kyr tuning

Edgar_Figure 6

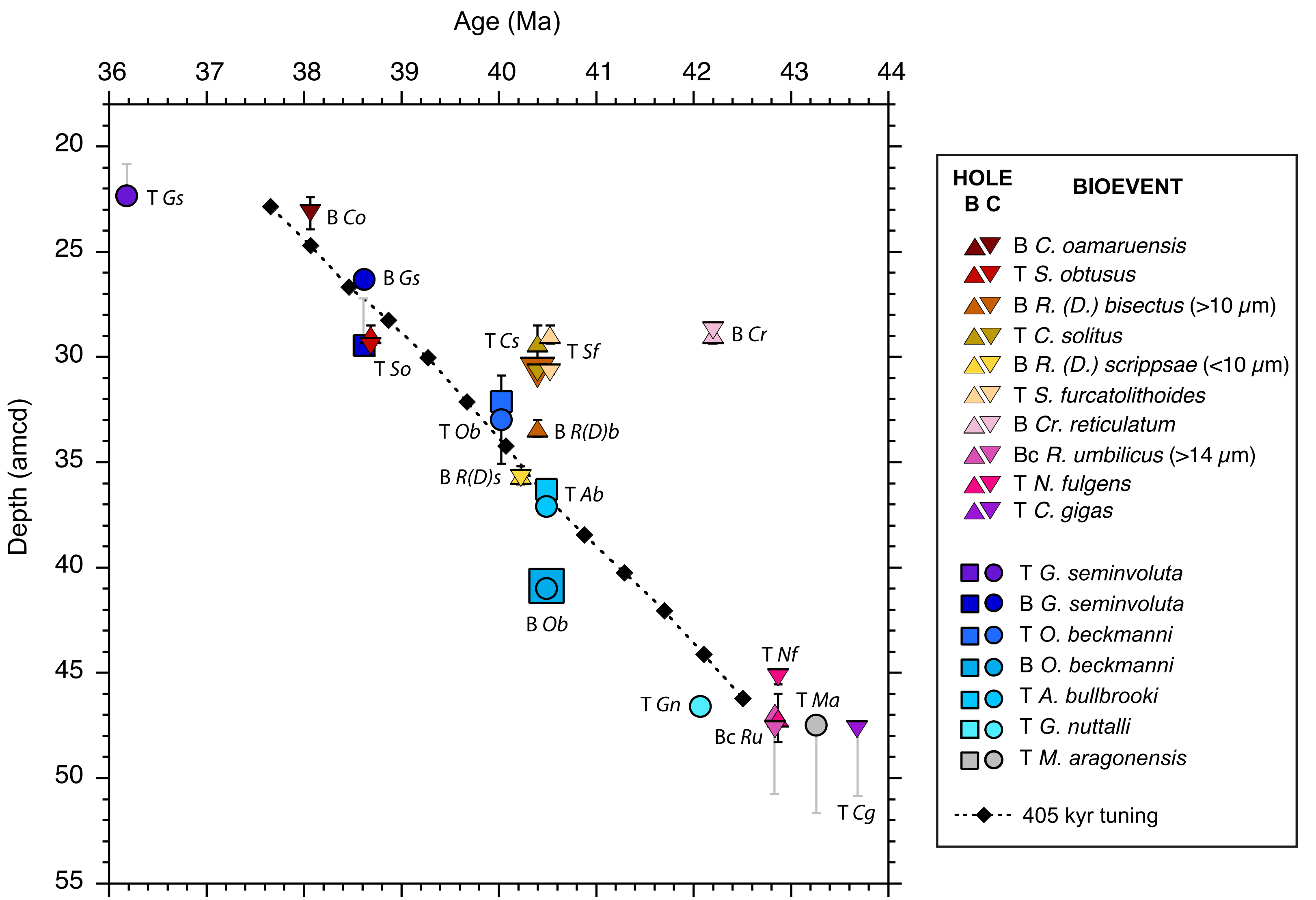

Table 1 - Composite depth offsets within splice, ODP Site 865

Hole	Core	Splice Offset (m)
865B	4H	0.78
865B	5H	2.28
865C	4H	0.00
865C	5H	3.22
865C	6H	3.46

Table 2 Splice tie points, ODP Site 865

Site, hole, core, section	Interval (cm)	Top of Section Depth (mbsf)	Depth (mbsf)	Splice offset (m)	Depth (mcd)	Correlation	Site, hole, core, section	Interval (cm)	Top of Section Depth (mbsf)	Depth (mbsf)	Splice offset (m)	Depth (mcd)
						start=>	865C-4H-1	4	22.30	22.34	0.00	22.34
865C-4H-6	20	29.80	30.00	0.00	30.00	tie to:	865B-4H-2	22	29.00	29.22	0.78	30.00
865B-4H-5	92	33.50	34.42	0.78	35.20	tie to:	865C-5H-1	18	31.80	31.98	3.22	35.20
865C-5H-5	122	37.80	39.02	3.22	42.24	tie to:	865B-5H-2	146	38.50	39.96	2.28	42.24
865B-5H-5	44	43.00	43.44	2.28	45.72	tie to:	865C-6H-1	96	41.30	42.26	3.46	45.72
865C-6H-2	141	42.80	44.21	3.46	47.67	<=end						

Table 3 - Mapping pairs for adjusting mcd to amcd, ODP Hole 865B

Site-Core-Type	Depth (mcd)	Offset Depth (amcd)
865B-4H	28.40	28.44
865B-4H	28.90	29.02
865B-4H	30.00	30.00
865B-4H	35.20	35.20
865B-4H	36.21	36.32
865B-5H	40.12	39.82
865B-5H	40.50	40.30
865B-5H	41.32	41.20
865B-5H	41.74	41.72
865B-5H	42.24	42.24
865B-5H	45.72	45.72
865B-5H	46.80	46.81

Table 4 - Mapping pairs for adjusting mcd to amcd, ODP Hole 865C

Core	Depth (mcd)	Offset Depth (amcd)
865C-4H	22.30	22.30
865C-4H	30.00	30.00
865C-4H	30.42	30.64
865C-5H	35.20	35.20
865C-5H	42.24	42.24
865C-5H	43.84	43.74
865C-6H	45.06	45.12
865C-6H	45.72	45.72
865C-6H	47.67	47.67

Table 5. Planktic foraminiferal datums in ODP Holes 865B and C

Event	Base of planktic foraminiferal Zone	GTS2012 Age (Ma)	Top sample	Top depth (mbsf)	Top depth (mcd)	Top depth (amcd)	Bottom sample	Bottom depth (mbsf)	Bottom depth (mcd)	Bottom depth (amcd)	Mid-point depth (amcd)	± (m)
HOLE B												
T *G. seminvoluta*	E15	36.18	3H-2, 75-77	20.25	-	-	3H-2, 95-97	20.45	-	-	-	-
B *G. seminvoluta*		38.62	3H-6, 110-112	26.60	-	-	4H-1, 110-112	28.62	29.40	29.47	-	-
T *O. beckmanni*	E13	40.03	4H-3, 80-82	31.30	32.08	32.08	4H-3,W, 90-92	31.42	32.20	32.20	32.14	0.06
T *A. bullbrooki*		40.49	4H-CC, 10-12	35.36	36.14	36.24	4H-CC, 20-22	35.48	36.26	36.36	36.30	0.06
B *O. beckmanni*	E12	40.49	5H-2, 20-22	38.70	40.98	40.83	5H-2, 30-32	38.82	41.10	40.96	40.89	0.07
B *G. index*		42.64	7H-4, 110-112	61.6	-	-	7H-5, 55-60	62.60	-	-	-	-
B *Mo. lehneri*		43.15	7H-2, 87-89	58.37	-	-	7H-3, 57-59	59.57	-	-	-	-
T *M. aragonensis*	E10	43.26	6H-1, 75-77	47.25	-	-	6H-2,75-77	48.77	-	-	-	-
HOLE C												
T *G. seminvoluta*	E15	36.18	3H-6, 46-48	20.76	20.76	-	4H-1, 5-7	22.37	22.37	22.37	-	-
B *G. seminvoluta*		38.62	4H-3, 95-97	26.25	26.25	26.25	4H-3, 110-112	26.42	26.42	26.42	26.34	0.07
T *O. beckmanni*	E13	40.03	4H-CC, 10-12	30.7	30.7	30.91	5H-1, 5-7	31.87	35.09	35.10	33.00	2.10
B *O. beckmanni*	E12	40.49	5H-4, 145-147	37.75	40.97	40.97	5H-5, 5-7	37.87	41.09	41.09	41.03	0.05
T *A. bullbrooki*		40.49	5H-2, 55-57	33.85	37.07	37.07	5H-2, 65-67	33.97	37.19	37.19	37.13	0.05
T *Gu. nuttalli*	E11	42.07	6H-2, 25-27	43.05	46.51	46.51	6H-2, 45-47	43.27	46.73	46.73	46.62	0.10
B *G. index*		42.64	7H-4, 110-112	56.4	-	-	7H-5, 70-72	57.52	-	-	-	-
B *Mo. lehneri*		43.15	7H-4, 110-112	56.4	-	-	7H-5, 70-72	57.52	-	-	-	-
T *M. aragonensis*	E10	43.26	6H-2, 125-127	44.05	47.51	47.51	7H-1, 110-112	51.92	-	-	-	-

T = Top; B = Base; A = *Acarinina;* G = *Globigerinatheka;* Gu = *Guembelitrioides;* M = *Morozovella;* Mo = *Morozovelloides*; O = *Orbulinoides*

Full sample window in which datum could fall is reported, i.e., top depth of top sample and lowermost depth in bottom sample.

Table 6. Calcareous nannofossil datums in ODP Holes 865B and C

Datum	Base of Nannofossil Zone	GTS2012 Age (Ma)	Top sample	Depth (mbsf)	Depth (mcd)	Depth (amcd)	Bottom sample	Depth (mbsf)	Depth (mcd)	Depth (amcd)	Mid point (amcd)	± (m)
HOLE B												
T *C. grandis*		**38.01**	3H-1, 70-72*	18.70	-	-	3H-1, 132*	19.32	-	-	-	-
B *C. oamaruensis*	NP18	**38.07**	3H-3, 110*	22.10	-	-	3H-4, 123*	23.23	-	-	-	-
T *S. obtusus*	CNE16	**38.69**	4H-1, 16*	27.66	28.44	28.49	4H-2, 40*	29.40	30.18	29.35	28.92	0.43
B R. (*D.) bisectus* (>10 µm)	CNE15	**40.40**	4H-4, 20-22	32.20	32.98	32.98	4H-4, 107*	33.07	33.85	33.76	33.37	0.39
T *C. solitus*	NP17	40.40	4H-1, 16*	27.66	28.44	28.49	4H-2, 40*	29.4	30.18	30.18	29.33	0.85
B R. *(D.) scrippsae* (<10 µm)		*40.23*	4H-5, 90-92	34.40	35.18	35.18	4H-5, 120*	34.70	35.48	36.04	35.61	0.43
T *S. furcatolithoides*		**40.53**	4H-1, 16*	27.66	28.44	28.49	4H-2, 40*	29.4	30.18	29.35	28.92	0.43
Bc *Cr. reticulatum*	CNE14	**42.20**	4H-1, 16*	27.66	28.44	28.49	4H-2, 40*	29.40	30.18	29.35	28.92	0.43
Bc *R. umbilicus* (>14 µm)	CNE13	**42.84**	5H-CC*	44.58	46.86	46.87	6H-1, 81-85*	47.35	-	-	-	-
T *N. fulgens*	NP16	42.87	5H-5, 70-72*	43.70	45.98	45.98	5H-6, 54-56*	44.56	46.84	46.85	46.42	1.15
B *R. umbilicus*		43.32	6H-1, 81-85*	47.31	-	-	6H-2, 73-75*	48.75	-	-	-	-
T *C. gigas*	CNE12; NP15c	**43.68**	6H-1, 81-85*	47.31	-	-	6H-2, 73-75*	48.75	-	-	-	-
HOLE C												
T *C. grandis*		**38.01**	3H-5, 80*	18.70	-	-	3H-6, 10-11*	20.41	-	-	-	-
B *C. oamaruensis*	NP18	**38.07**	4H-1, 10-11*	22.40	22.40	22.40	4H-2, 10-11*	23.91	23.91	23.91	23.15	0.76
T *S. obtusus*	CNE16	**38.69**	4H-5, 75-77	29.05	29.05	29.05	4H-6, 10-11*	29.91	29.91	29.91	29.48	0.43
B R. (*D.) bisectus* (>10 µm)	CNE15	**40.40**	4H-6, 65-67	30.45	30.45	30.67	4H-CC*	30.6	30.60	30.81	30.74	0.07
T *C. solitus*	NP17	40.40	4H-6, 65-67	30.45	30.45	30.67	4H-CC	30.6	30.60	30.81	30.74	0.07
B R. *(D.) scrippsae* (<10 µm)		*40.23*	5H-1, 45-47	32.25	35.47	35.47	5H-1, 95-97	32.77	35.99	35.99	35.73	0.26
T *S. furcatolithoides*		**40.53**	4H-6, 65-67	30.45	30.45	30.67	4H-CC	30.6	30.60	30.81	30.74	0.07
Bc *Cr. reticulatum*	CNE14	**42.20**	4H-5, 10-11*	28.40	28.40	28.40	4H-5, 75-77	29.07	29.07	29.07	28.73	0.34
Bc *R. umbilicus* (>14 µm)	CNE13	**42.84**	6H-CC*	44.22	47.68	47.68	7H-1, 10-11*	50.91	-	-	-	-
T *N. fulgens*	NP16	42.87	6H-1, 10-11*	41.40	44.86	44.89	6H-1, 75*	42.05	45.51	45.53	45.21	0.32
B *R. umbilicus*		43.32	7H-2, 10-11*	52.40	-	-	7H-2, 100*	53.3	-	-	-	-
T *C. gigas*	CNE12; NP15c	**43.68**	6H-CC*	44.22	47.68	47.68	7H-1,10-11*	50.91	-	-	-	-

T = Top; B = Base; C = Chiasmolithus; Cr = Cribrocentrum; D = Dictyococcites; N = Nannotetrina; R = Reticulofenestra; S = Sphenolithus;* = From Bralower and Mutterlose (1995)

All ages on the GTS2012 timescale from Gradstein *et al.* (2012) with those in bold recalculated based on revised calibrations from Agnini *et al.* (2014), in italics from Bohaty *et al*. (2009).

Calcareous nannofossil zones: NP Zones are from Martini (1971) and CNE Zones are from Agnini *et al*. (2014)

Edgar_Fig S1

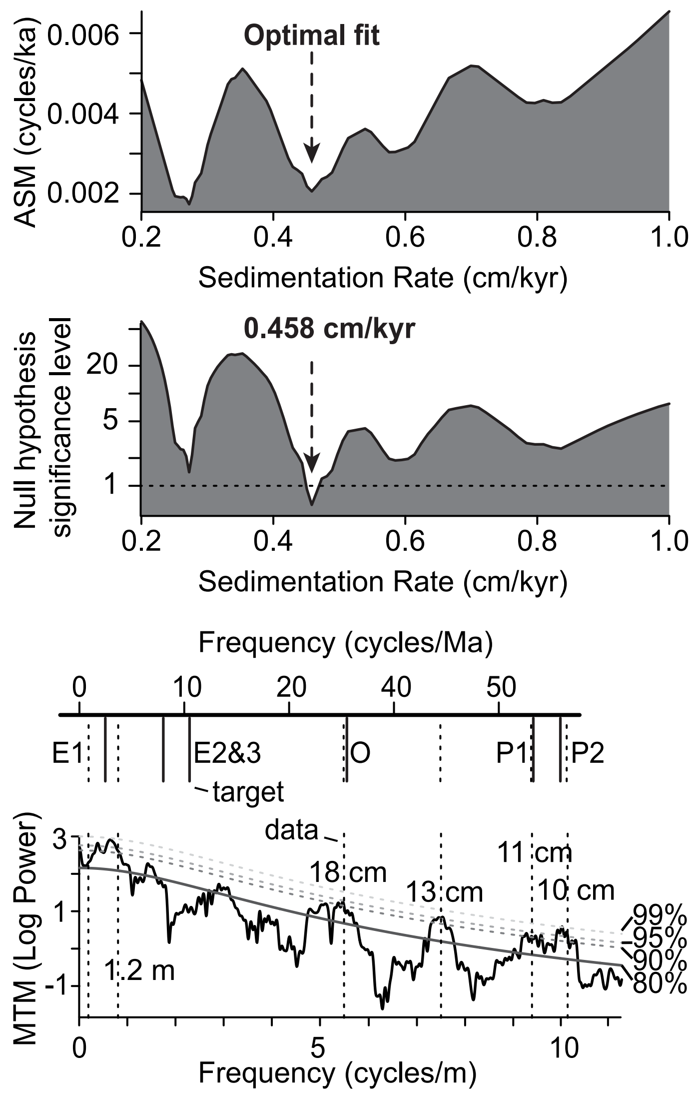

ASM (cycles/ka)
0.006
0.004
0.002
Optimal fit
0.2
0.4
0.6
0.8
1.0
Sedimentation Rate (cm/kyr)
Null hypothesis significance level
20
5
1
0.458 cm/kyr
0.2
0.4
0.6
0.8
1.0
Sedimentation Rate (cm/kyr)
Frequency (cycles/Ma)
0
10
20
40
50
E1
E2&3
O
P1
P2
target
data
MTM (Log Power)
3
1
-1
1.2 m
18 cm
13 cm
11 cm
10 cm
99%
95%
90%
80%
0
5
10
Frequency (cycles/m)

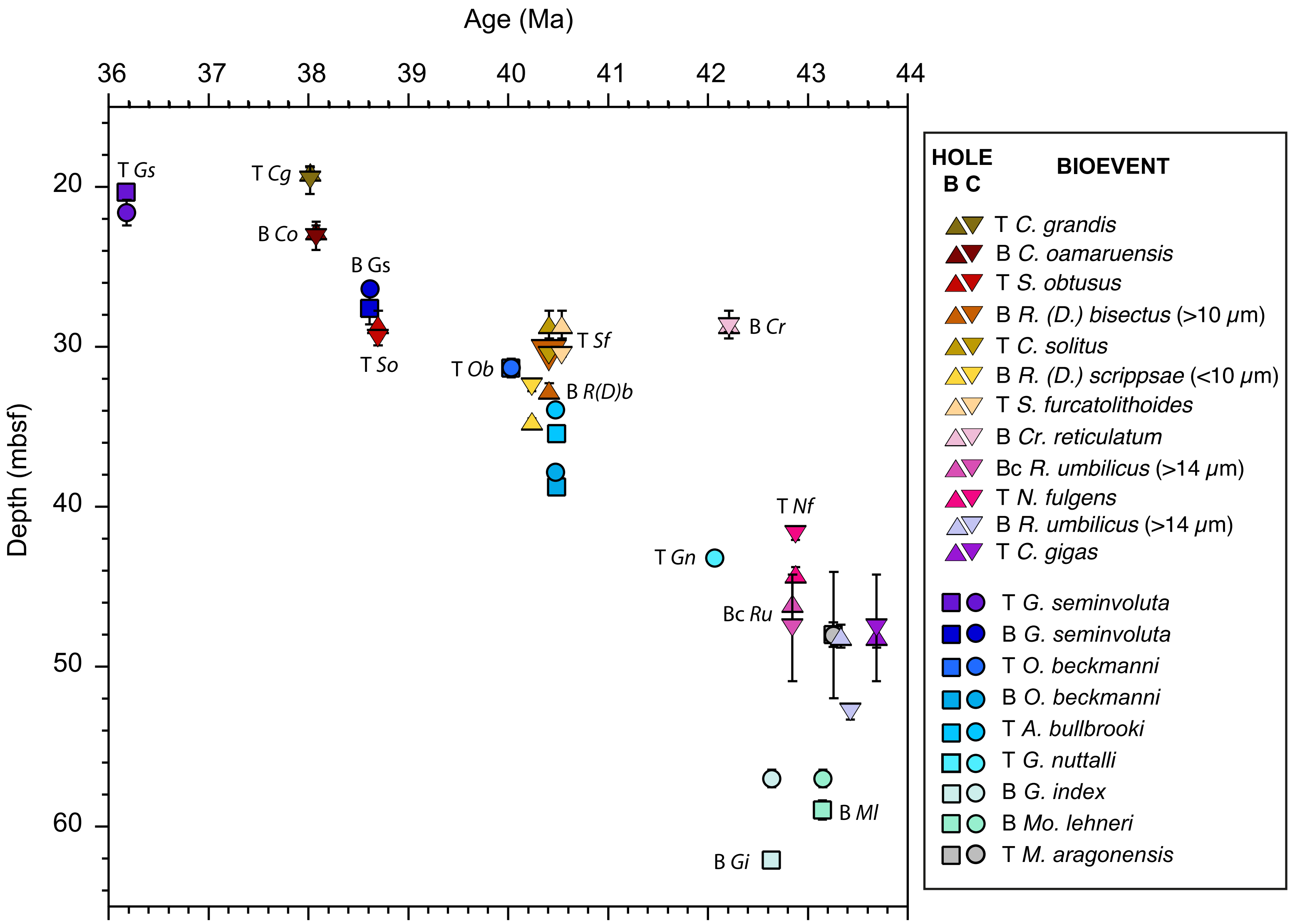
Age (Ma)
36
37
38
39
40
41
42
43
44
Depth (mbsf)
20
30
40
50
60
T Gs
T Cg
B Co
B Gs
T So
T Ob
T Sf
B R(D)b
B Cr
T Nf
T Gn
Bc Ru
B Ml
B Gi
HOLE
B C
BIOEVENT
T C. grandis
B C. oamaruensis
T S. obtusus
B R. (D.) bisectus (>10 µm)
T C. solitus
B R. (D.) scrippsae (<10 µm)
T S. furcatolithoides
B Cr. reticulatum
Bc R. umbilicus (>14 µm)
T N. fulgens
B R. umbilicus (>14 µm)
T C. gigas
T G. seminvoluta
B G. seminvoluta
T O. beckmanni
B O. beckmanni
T A. bullbrooki
T G. nuttalli
B G. index
B Mo. lehneri
T M. aragonensis

Supplementary Table 2. Benthic foraminifera *Nuttallides truempyi* stable isotope data for ODP Hole 865B from the 250-300 µm sieve size fraction

Site	Hole	Core	Type	Section	Half	Top (cm)	Bottom (cm)	Depth (mbsf)	Splice offset (m)	Depth (mcd)	Adjusted Composite Depth (amcd)	Orbitally-tuned Age (Ma; GTS2012)	Coarse fraction (>63 µm, %)	δ13C (per mil, VPDB)	δ18O (per mil, VPDB)
865	B	4	H	3	W	10	12	30.60	0.78	31.38	31.380	39.531	35.98	0.420	0.850
865	B	4	H	3	W	20	22	30.70	0.78	31.48	31.480	39.550	37.07	0.420	0.850
865	B	4	H	3	W	30	32	30.80	0.78	31.58	31.580	39.568	34.51	0.190	0.801
865	B	4	H	3	W	40	42	30.90	0.78	31.68	31.680	39.587	32.82	0.260	0.780
865	B	4	H	3	W	50	52	31.00	0.78	31.78	31.780	39.606	29.66	0.273	0.859
865	B	4	H	3	W	58	62	31.08	0.78	31.86	31.860	39.621	28.74	0.308	0.709
865	B	4	H	3	W	70	72	31.20	0.78	31.98	31.980	39.644	30.14	0.283	0.691
865	B	4	H	3	W	80	82	31.30	0.78	32.08	32.080	39.663	28.64	0.316	0.881
865	B	4	H	3	W	90	92	31.40	0.78	32.18	32.180	39.682	29.06	0.432	0.839
865	B	4	H	3	W	98	102	31.48	0.78	32.26	32.260	39.697	31.50	0.329	0.933
865	B	4	H	3	W	110	112	31.60	0.78	32.38	32.380	39.720	26.40	0.185	0.634
865	B	4	H	3	W	120	122	31.70	0.78	32.48	32.480	39.739	27.29	0.419	0.885
865	B	4	H	3	W	130	132	31.80	0.78	32.58	32.580	39.758	32.04	0.318	0.745
865	B	4	H	3	W	140	142	31.90	0.78	32.68	32.680	39.777	35.03	0.296	0.615
865	B	4	H	3	W	148	150	31.98	0.78	32.76	32.760	39.793	33.52	0.266	0.690
865	B	4	H	4	W	8	12	32.08	0.78	32.86	32.860	39.812	32.46	0.578	0.535
865	B	4	H	4	W	20	22	32.20	0.78	32.98	32.980	39.835	34.05	0.315	0.564
865	B	4	H	4	W	30	32	32.30	0.78	33.08	33.080	39.854	35.80	0.491	0.737
865	B	4	H	4	W	40	42	32.40	0.78	33.18	33.180	39.873	34.18	0.501	0.625
865	B	4	H	4	W	48	50	32.48	0.78	33.26	33.260	39.888	35.82	0.571	0.658
865	B	4	H	4	W	60	62	32.60	0.78	33.38	33.380	39.911	37.69	0.459	0.629
865	B	4	H	4	W	70	72	32.70	0.78	33.48	33.480	39.931	32.72	0.405	0.468
865	B	4	H	4	W	80	82	32.80	0.78	33.58	33.580	39.950	33.91	0.450	0.594
865	B	4	H	4	W	88	92	32.88	0.78	33.66	33.660	39.965	28.53	0.453	0.650
865	B	4	H	4	W	98	100	32.98	0.78	33.76	33.760	39.984	28.51	0.294	0.466
865	B	4	H	4	W	110	112	33.10	0.78	33.88	33.880	40.007	28.66	0.445	0.591
865	B	4	H	4	W	120	122	33.20	0.78	33.98	33.980	40.026	26.18	0.503	0.528

865	B	4	H	4	W	130	132	33.30	0.78	34.08	34.080	40.045	27.00	0.528	0.633
865	B	4	H	4	W	140	142	33.40	0.78	34.18	34.180	40.065	28.55	0.618	0.671
865	B	4	H	4	W	148	150	33.48	0.78	34.26	34.260	40.079	27.69	0.341	0.608
865	B	4	H	5	W	10	12	33.60	0.78	34.38	34.380	40.100	31.31	0.289	0.631
865	B	4	H	5	W	20	22	33.70	0.78	34.48	34.480	40.117	30.32	0.593	0.643
865	B	4	H	5	W	30	32	33.80	0.78	34.58	34.580	40.134	27.02	0.647	0.464
865	B	4	H	5	W	40	42	33.90	0.78	34.68	34.680	40.151	26.59	0.570	0.459
865	B	4	H	5	W	50	52	34.00	0.78	34.78	34.780	40.169	26.77	0.453	0.595
865	B	4	H	5	W	60	62	34.10	0.78	34.88	34.880	40.186	28.04	0.443	0.822
865	B	4	H	5	W	70	72	34.20	0.78	34.98	34.980	40.203	26.37	0.398	0.376
865	B	4	H	5	W	80	82	34.30	0.78	35.08	35.080	40.220	32.21	0.345	0.500
865	B	4	H	5	W	90	92	34.40	0.78	35.18	35.180	40.237	28.22	0.299	0.441
865	B	4	H	5	W	100	104	34.50	0.78	35.28	35.289	40.256	25.93	0.276	0.446
865	B	4	H	5	W	110	112	34.60	0.78	35.38	35.400	40.275	24.41	0.359	0.476
865	B	4	H	5	W	120	122	34.70	0.78	35.48	35.510	40.294	23.85	0.197	0.338
865	B	4	H	5	W	130	132	34.80	0.78	35.58	35.621	40.313	23.05	0.278	0.571
865	B	4	H	5	W	140	142	34.90	0.78	35.68	35.732	40.332	25.94	0.333	0.708
865	B	4	H	6	W	10	12	35.10	0.78	35.88	35.954	40.370	23.94	0.321	0.730
865	B	4	H	6	W	18	20	35.18	0.78	35.96	36.043	40.385	21.21	0.259	0.917
865	B	4	H	CC	W	10	12	35.36	0.78	36.14	36.242	40.419	20.39	0.171	1.013
865	B	4	H	CC	W	20	22	35.46	0.78	36.24	36.347	40.437	19.73	0.210	1.090
865	B	4	H	CC	W	30	32	35.56	0.78	36.34	36.436	40.452	21.12	0.110	0.742
865	B	5	H	1	W	2	4	37.02	2.28	39.30	39.086	41.022	16.64	0.277	0.879
865	B	5	H	1	W	10	12	37.10	2.28	39.38	39.158	41.038	17.95	0.330	0.938
865	B	5	H	1	W	20	22	37.20	2.28	39.48	39.247	41.058	17.02	0.316	0.968
865	B	5	H	1	W	30	32	37.30	2.28	39.58	39.337	41.079	17.19	0.264	0.790
865	B	5	H	1	W	38	40	37.38	2.28	39.66	39.408	41.095	17.61	0.257	0.799
865	B	5	H	1	W	50	52	37.50	2.28	39.78	39.516	41.119	16.19	0.263	0.869
865	B	5	H	1	W	60	62	37.60	2.28	39.88	39.605	41.140	18.57	0.290	0.898
865	B	5	H	1	W	70	72	37.70	2.28	39.98	39.695	41.160	17.32	0.355	0.831
865	B	5	H	1	W	80	82	37.80	2.28	40.08	39.784	41.181	19.40	0.269	0.745
865	B	5	H	1	W	90	92	37.90	2.28	40.18	39.896	41.206	16.47	0.286	0.797
865	B	5	H	1	W	100	104	38.00	2.28	40.28	40.022	41.235	20.05	0.233	0.679
865	B	5	H	1	W	110	112	38.10	2.28	40.38	40.148	41.264	16.20	0.235	0.828
865	B	5	H	1	W	120	122	38.20	2.28	40.48	40.275	41.292	15.65	0.330	0.792
865	B	5	H	1	W	127	129	38.27	2.28	40.55	40.355	41.311	17.22	0.392	0.904
865	B	5	H	1	W	140	142	38.40	2.28	40.68	40.498	41.344	16.52	0.266	0.869

865	B	5	H	1	W	148	150	38.48	2.28	40.76	40.585	41.364	15.34	0.304	0.772
865	B	5	H	2	W	0	2	38.50	2.28	40.78	40.607	41.369	13.69	0.221	0.769
865	B	5	H	2	W	10	12	38.60	2.28	40.88	40.717	41.394	13.56	0.335	0.851
865	B	5	H	2	W	20	22	38.70	2.28	40.98	40.827	41.419	12.14	0.350	0.942
865	B	5	H	2	W	30	32	38.80	2.28	41.08	40.937	41.445	13.51	0.351	0.813
865	B	5	H	2	W	40	42	38.90	2.28	41.18	41.046	41.470	13.57	0.394	0.938
865	B	5	H	2	W	50	52	39.00	2.28	41.28	41.156	41.495	12.28	0.311	0.845
865	B	5	H	2	W	60	62	39.10	2.28	41.38	41.274	41.522	13.51	0.270	0.631
865	B	5	H	2	W	70	72	39.20	2.28	41.48	41.398	41.551	12.30	0.371	0.830
865	B	5	H	2	W	80	82	39.30	2.28	41.58	41.522	41.579	13.61	0.252	0.778
865	B	5	H	2	W	90	92	39.40	2.28	41.68	41.646	41.608	13.82	0.288	0.805
865	B	5	H	2	W	100	104	39.50	2.28	41.78	41.762	41.634	15.22	0.290	0.775
865	B	5	H	2	W	110	112	39.60	2.28	41.88	41.866	41.658	11.80	0.305	0.778
865	B	5	H	2	W	120	122	39.70	2.28	41.98	41.970	41.682	14.29	0.329	0.824
865	B	5	H	2	W	130	132	39.80	2.28	42.08	42.074	41.706	14.11	0.259	0.788
865	B	5	H	2	W	140	142	39.90	2.28	42.18	42.178	41.726	11.64	0.379	0.881
865	B	5	H	2	W	148	150	39.98	2.28	42.26	42.260	41.742	11.29	0.319	0.821

Supplementary Table 3. Benthic foraminifera *Nuttallides truempyi* stable isotope data for ODP Hole 865C from the 250-300 µm sieve size fraction

Site	Hole	Core	Type	Section	Half	Top (cm)	Bottom (cm)	Depth (mbsf)	Splice offset (m)	Depth (mcd)	Adjusted Composite Depth (amcd)	Orbitally-tuned Age (Ma; GTS2012)	Coarse fraction (>63 µm, %)	δ13C (per mil, VPDB)	δ18O (per mil, VPDB)
865	C	4	H	2	W	65	67	24.45	0.00	24.45	24.450	38.010	11.35	0.042	1.179
865	C	4	H	2	W	85	87	24.65	0.00	24.65	24.650	38.054	12.95	0.136	1.151
865	C	4	H	2	W	95	97	24.75	0.00	24.75	24.750	38.076	11.01	0.275	1.114
865	C	4	H	2	W	110	112	24.91	0.00	24.91	24.910	38.108	-	0.172	0.959
865	C	4	H	2	W	115	117	24.95	0.00	24.95	24.950	38.116	13.23	0.402	1.015
865	C	4	H	3	W	5	7	25.35	0.00	25.35	25.350	38.197	20.08	0.317	1.155
865	C	4	H	3	W	25	27	25.55	0.00	25.55	25.550	38.238	14.70	0.401	0.950
865	C	4	H	3	W	45	47	25.75	0.00	25.75	25.750	38.278	13.69	0.333	0.998
865	C	4	H	3	W	85	87	26.15	0.00	26.15	26.150	38.359	12.85	0.475	0.870
865	C	4	H	3	W	110	112	26.41	0.00	26.41	26.410	38.411	-	0.195	1.075
865	C	4	H	3	W	135	137	26.65	0.00	26.65	26.650	38.460	14.28	0.773	1.158
865	C	4	H	4	W	5	7	26.85	0.00	26.85	26.850	38.510	13.05	0.217	0.949
865	C	4	H	4	W	25	27	27.05	0.00	27.05	27.050	38.561	16.67	0.443	1.134
865	C	4	H	4	W	50	52	27.30	0.00	27.30	27.300	38.625	18.64	0.118	0.764
865	C	4	H	4	W	70	72	27.50	0.00	27.50	27.500	38.676	19.94	0.324	0.972
865	C	4	H	4	W	90	92	27.70	0.00	27.70	27.700	38.727	20.82	0.208	0.876
865	C	4	H	4	W	112	114	27.92	0.00	27.92	27.920	38.784	22.34	0.309	0.938
865	C	4	H	4	W	131	133	28.11	0.00	28.11	28.110	38.833	19.61	0.279	0.937
865	C	4	H	5	W	5	7	28.35	0.00	28.35	28.350	38.892	30.63	0.243	0.948
865	C	4	H	5	W	15	17	28.45	0.00	28.45	28.450	38.914	19.73	0.684	0.524
865	C	4	H	5	W	15	17	28.45	0.00	28.45	28.450	38.914	-	0.141	0.820
865	C	4	H	5	W	25	27	28.55	0.00	28.55	28.550	38.937	27.04	0.239	0.859

865	C	4	H	5	W	35	37	28.65	0.00	28.65	28.650	38.960	25.99	0.101	0.933
865	C	4	H	5	W	45	47	28.75	0.00	28.75	28.750	38.983	27.30	0.141	0.820
865	C	4	H	5	W	65	67	28.95	0.00	28.95	28.950	39.029	24.10	0.225	0.833
865	C	4	H	5	W	75	77	29.05	0.00	29.05	29.050	39.052	25.44	0.094	0.835
865	C	4	H	5	W	85	87	29.15	0.00	29.15	29.150	39.075	19.99	0.223	0.694
865	C	4	H	5	W	95	97	29.25	0.00	29.25	29.250	39.097	24.35	0.106	0.673
865	C	4	H	5	W	105	107	29.35	0.00	29.35	29.350	39.120	26.16	0.286	0.918
865	C	4	H	5	W	110	112	29.41	0.00	29.41	29.410	39.134	-	0.272	0.752
865	C	4	H	5	W	115	117	29.45	0.00	29.45	29.450	39.143	24.27	0.120	0.787
865	C	4	H	5	W	125	127	29.55	0.00	29.55	29.550	39.166	26.11	0.187	0.819
865	C	4	H	5	W	135	137	29.65	0.00	29.65	29.650	39.189	25.38	0.130	0.762
865	C	4	H	5	W	135	137	29.65	0.00	29.65	29.650	39.189	25.38	0.079	0.716
865	C	4	H	5	W	144	146	29.74	0.00	29.74	29.740	39.209	28.65	0.275	0.783
865	C	4	H	6	W	5	7	29.85	0.00	29.85	29.850	39.235	25.64	0.072	0.767
865	C	4	H	6	W	15	17	29.95	0.00	29.95	29.950	39.257	20.96	0.413	0.760
865	C	4	H	6	W	25	27	30.05	0.00	30.05	30.076	39.285	24.03	0.040	0.749
865	C	4	H	6	W	35	37	30.15	0.00	30.15	30.229	39.314	26.28	0.274	0.753
865	C	4	H	6	W	45	47	30.25	0.00	30.25	30.381	39.342	23.63	0.039	0.743
865	C	4	H	6	W	55	57	30.35	0.00	30.35	30.533	39.371	23.94	0.302	0.827
865	C	4	H	6	W	63	65	30.44	0.00	30.44	30.659	39.395	-	0.166	0.661
865	C	4	H	6	W	65	67	30.45	0.00	30.45	30.669	39.397	28.23	0.313	0.895
865	C	4	H	6	W	75	77	30.55	0.00	30.55	30.764	39.415	34.14	0.251	0.835
865	C	5	H	1	W	5	7	31.85	3.22	35.07	35.076	40.219	25.71	0.213	0.365
865	C	5	H	1	W	15	17	31.95	3.22	35.17	35.171	40.236	28.98	0.395	0.294
865	C	5	H	1	W	25	27	32.05	3.22	35.27	35.270	40.252	24.04	0.380	0.343
865	C	5	H	1	W	35	37	32.15	3.22	35.37	35.370	40.270	17.04	0.252	0.290
865	C	5	H	1	W	45	47	32.25	3.22	35.47	35.470	40.287	21.30	0.292	0.324
865	C	5	H	1	W	55	57	32.35	3.22	35.57	35.570	40.304	17.34	0.285	0.520
865	C	5	H	1	W	63	65	32.44	3.22	35.66	35.660	40.319	-	0.044	0.632

865	C	5	H	1	W	65	67	32.45	3.22	35.67	35.670	40.321	21.74	0.325	0.469
865	C	5	H	1	W	75	77	32.55	3.22	35.77	35.770	40.338	19.14	0.207	0.621
865	C	5	H	1	W	85	87	32.65	3.22	35.87	35.870	40.355	24.03	0.417	0.755
865	C	5	H	1	W	95	97	32.75	3.22	35.97	35.970	40.372	19.13	0.082	0.653
865	C	5	H	1	W	105	107	32.85	3.22	36.07	36.070	40.389	19.62	0.268	0.859
865	C	5	H	1	W	115	117	32.95	3.22	36.17	36.170	40.407	15.61	0.127	0.725
865	C	5	H	1	W	125	127	33.05	3.22	36.27	36.270	40.424	14.59	0.076	0.712
865	C	5	H	1	W	135	137	33.15	3.22	36.37	36.370	40.441	15.48	0.125	0.770
865	C	5	H	1	W	145	147	33.25	3.22	36.47	36.470	40.458	15.11	0.045	0.616
865	C	5	H	2	W	5	7	33.35	3.22	36.57	36.570	40.476	13.47	0.055	0.727
865	C	5	H	2	W	15	17	33.45	3.22	36.67	36.670	40.498	17.54	0.060	0.771
865	C	5	H	2	W	25	27	33.55	3.22	36.77	36.770	40.519	13.46	0.072	0.869
865	C	5	H	2	W	35	37	33.65	3.22	36.87	36.870	40.540	15.43	-0.070	0.806
865	C	5	H	2	W	45	47	33.75	3.22	36.97	36.970	40.562	11.93	-0.324	0.679
865	C	5	H	2	W	55	57	33.85	3.22	37.07	37.070	40.583	16.03	0.050	0.707
865	C	5	H	2	W	65	67	33.95	3.22	37.17	37.170	40.604	13.65	0.105	0.671
865	C	5	H	2	W	75	77	34.05	3.22	37.27	37.270	40.626	17.29	0.196	0.770
865	C	5	H	2	W	85	87	34.15	3.22	37.37	37.370	40.647	14.06	0.104	0.673
865	C	5	H	2	W	95	97	34.25	3.22	37.47	37.470	40.668	16.85	0.064	0.707
865	C	5	H	2	W	105	107	34.35	3.22	37.57	37.570	40.689	13.05	0.046	0.753
865	C	5	H	2	W	115	117	34.45	3.22	37.67	37.670	40.711	17.56	0.299	0.572
865	C	5	H	2	W	125	127	34.55	3.22	37.77	37.770	40.732	14.57	0.172	0.637
865	C	5	H	2	W	135	137	34.65	3.22	37.87	37.870	40.753	16.85	0.159	0.729
865	C	5	H	2	W	145	147	34.75	3.22	37.97	37.970	40.775	13.95	0.210	0.702
865	C	5	H	3	W	5	7	34.85	3.22	38.07	38.07	40.796	18.25	0.161	0.750
865	C	5	H	3	W	15	17	34.95	3.22	38.17	38.170	40.817	12.37	0.179	0.639
865	C	5	H	3	W	25	27	35.05	3.22	38.27	38.270	40.839	15.74	0.214	0.685
865	C	5	H	3	W	35	37	35.15	3.22	38.37	38.370	40.860	12.88	0.157	0.803
865	C	5	H	3	W	47	49	35.27	3.22	38.49	38.490	40.886	17.06	0.258	0.684

865	C	5	H	3	W	55	57	35.35	3.22	38.57	38.570	40.904	13.12	0.153	0.695
865	C	5	H	3	W	63	65	35.44	3.22	38.66	38.660	40.925	-	0.255	0.871
865	C	5	H	3	W	65	67	35.45	3.22	38.67	38.670	40.927	16.06	0.267	0.683
865	C	5	H	3	W	75	77	35.55	3.22	38.77	38.770	40.950	14.32	0.096	0.555
865	C	5	H	3	W	85	87	35.65	3.22	38.87	38.870	40.972	16.11	0.352	0.827
865	C	5	H	3	W	95	97	35.75	3.22	38.97	38.970	40.995	14.07	0.151	0.887
865	C	5	H	3	W	105	107	35.85	3.22	39.07	39.070	41.018	17.51	0.425	0.700
865	C	5	H	3	W	115	117	35.95	3.22	39.17	39.170	41.041	14.98	0.075	0.689
865	C	5	H	3	W	125	127	36.05	3.22	39.27	39.270	41.063	16.69	0.257	0.857
865	C	5	H	3	W	135	137	36.15	3.22	39.37	39.370	41.086	13.98	0.241	0.741
865	C	5	H	3	W	145	147	36.25	3.22	39.47	39.470	41.109	16.83	0.284	0.812
865	C	5	H	4	W	5	7	36.35	3.22	39.57	39.570	41.132	14.81	0.152	0.705
865	C	5	H	4	W	15	17	36.45	3.22	39.67	39.670	41.155	19.05	0.412	0.585
865	C	5	H	4	W	25	27	36.55	3.22	39.77	39.770	41.177	15.65	0.208	0.704
865	C	5	H	4	W	35	37	36.65	3.22	39.87	39.870	41.200	18.26	0.310	0.734
865	C	5	H	4	W	45	47	36.75	3.22	39.97	39.970	41.223	13.12	0.267	0.820
865	C	5	H	4	W	55	57	36.85	3.22	40.07	40.070	41.246	15.50	0.191	0.618
865	C	5	H	4	W	63	65	36.94	3.22	40.16	40.160	41.266	-	0.269	0.843
865	C	5	H	4	W	65	67	36.95	3.22	40.17	40.170	41.269	12.97	0.290	0.780
865	C	5	H	4	W	75	77	37.05	3.22	40.27	40.270	41.291	16.16	0.329	0.735
865	C	5	H	4	W	85	87	37.15	3.22	40.37	40.370	41.314	14.40	0.287	0.757
865	C	5	H	4	W	95	97	37.25	3.22	40.47	40.470	41.337	14.32	0.243	0.743
865	C	5	H	4	W	105	107	37.35	3.22	40.57	40.570	41.360	12.31	0.140	0.731
865	C	5	H	4	W	115	117	37.45	3.22	40.67	40.670	41.383	13.72	0.279	0.821
865	C	5	H	4	W	125	127	37.55	3.22	40.77	40.770	41.406	11.35	0.262	0.708
865	C	5	H	4	W	135	137	37.65	3.22	40.87	40.870	41.429	16.01	0.278	0.651
865	C	5	H	4	W	145	147	37.75	3.22	40.97	40.970	41.452	11.96	0.195	0.804
865	C	5	H	5	W	5	7	37.85	3.22	41.07	41.070	41.475	20.61	0.303	0.686
865	C	5	H	5	W	15	17	37.95	3.22	41.17	41.170	41.498	12.77	0.307	0.809

865	C	5	H	5	W	25	27	38.05	3.22	41.27	41.270	41.521	19.35	0.394	0.718
865	C	5	H	5	W	35	37	38.15	3.22	41.37	41.370	41.544	12.29	0.200	0.705
865	C	5	H	5	W	45	47	38.25	3.22	41.47	41.470	41.567	18.22	0.213	0.577
865	C	5	H	5	W	55	57	38.35	3.22	41.57	41.570	41.590	12.97	0.176	0.714
865	C	5	H	5	W	65	67	38.45	3.22	41.67	41.670	41.613	19.39	0.208	0.623
865	C	5	H	5	W	75	77	38.55	3.22	41.77	41.770	41.636	14.31	0.198	0.760
865	C	5	H	5	W	85	87	38.65	3.22	41.87	41.870	41.659	18.95	0.211	0.675
865	C	5	H	5	W	95	97	38.75	3.22	41.97	41.970	41.682	14.08	0.277	0.802
865	C	5	H	5	W	105	107	38.85	3.22	42.07	42.070	41.705	18.41	0.357	0.565
865	C	5	H	5	W	113	116	38.95	3.22	42.17	42.165	41.724	10.54	0.281	0.840
865	C	5	H	5	W	115	117	38.96	3.22	42.18	42.180	41.727	10.73	0.142	0.583
865	C	5	H	5	W	125	127	39.05	3.22	42.27	42.268	41.744	17.77	0.303	0.636
865	C	5	H	5	W	135	137	39.15	3.22	42.37	42.362	41.762	12.60	0.236	0.710
865	C	5	H	5	W	145	147	39.25	3.22	42.47	42.456	41.781	17.73	0.271	0.654
865	C	5	H	6	W	5	7	39.35	3.22	42.57	42.549	41.799	11.00	0.218	0.635
865	C	5	H	6	W	15	17	39.45	3.22	42.67	42.643	41.817	18.24	0.271	0.598
865	C	5	H	6	W	25	27	39.55	3.22	42.77	42.737	41.836	13.01	0.194	0.571
865	C	5	H	6	W	35	37	39.65	3.22	42.87	42.831	41.854	17.63	0.164	0.477
865	C	5	H	6	W	45	47	39.75	3.22	42.97	42.924	41.873	12.46	0.114	0.472
865	C	5	H	6	W	55	57	39.85	3.22	43.07	43.018	41.891	12.88	0.217	0.569
865	C	5	H	6	W	65	67	39.95	3.22	43.17	43.112	41.909	8.59	0.160	0.440
865	C	5	H	6	W	70	72	40.01	3.22	43.23	43.168	41.920	-	-0.081	0.312
865	C	5	H	6	W	75	77	40.05	3.22	43.27	43.206	41.928	14.49	0.130	0.390
865	C	5	H	6	W	85	87	40.15	3.22	43.37	43.299	41.946	13.46	0.166	0.478
865	C	5	H	6	W	95	97	40.25	3.22	43.47	43.393	41.964	15.21	0.249	0.450
865	C	5	H	CC	W	20	22	40.54	3.22	43.76	43.665	42.018	10.23	0.146	0.455
865	C	6	H	1	W	15	17	41.45	3.46	44.91	44.950	42.265	12.25	0.349	0.523
865	C	6	H	1	W	35	37	41.65	3.46	45.11	45.165	42.306	13.16	0.253	0.484
865	C	6	H	1	W	55	57	41.85	3.46	45.31	45.347	42.340	14.44	0.394	0.789

865	C	6	H	1	W	75	77	42.05	3.46	45.51	45.529	42.375	11.53	0.244	0.548
865	C	6	H	1	W	95	97	42.25	3.46	45.71	45.711	42.409	11.96	0.366	0.727
865	C	6	H	1	W	115	117	42.45	3.46	45.91	45.910	42.447	10.64	0.264	0.513
865	C	6	H	1	W	135	137	42.65	3.46	46.11	46.110	42.485	15.75	0.365	0.691
865	C	6	H	2	W	5	7	42.85	3.46	46.31	46.310		10.40	0.285	0.612
865	C	6	H	2	W	25	27	43.05	3.46	46.51	46.510		13.11	-0.062	0.493
865	C	6	H	2	W	45	47	43.25	3.46	46.71	46.710		14.32	0.206	0.709
865	C	6	H	2	W	63	65	43.43	3.46	46.89	46.890		14.44	0.293	0.785
865	C	6	H	2	W	125	127	44.05	3.46	47.51	47.510		12.72	0.195	0.760

NB. Samples with no coarse fraction data are shipboard samples

Supplementary Table 5. Tuning tie-points

405 kyr minima in La2011	Depth of ln Sr/Ca filtered maxima (amcd)	Sedimentation rate (cm/kyr)
37.255		
37.657	22.86	
38.07	24.72	0.450
38.466	26.68	0.495
38.871	28.26	0.390
39.278	30.04	0.437
39.674	32.14	0.530
40.076	34.24	0.522
40.47	36.54	0.584
40.879	38.46	0.469
41.289	40.26	0.439
41.703	42.06	0.435
42.107	44.12	0.510
42.506	46.22	0.526
42.912		